Numerical and Asymptotic Solutions of the Pridmore-Brown Equation

Sjoerd W. Rienstra*
Eindhoven University of Technology, 5612 AE Eindhoven, The Netherlands

https://doi.org/10.2514/1.J059140

A study is made of acoustic duct modes in two-dimensional and axisymmetric three-dimensional lined ducts with an isentropic inviscid transversely nonuniform mean flow and sound speed. These modes are described by a one-dimensional eigenvalue problem consisting of a Pridmore-Brown equation complemented by hard-wall or impedance-wall boundary conditions. A numerical solution, based on a Galerkin projection and an efficient method for the resulting nonlinear eigenvalue problem, is compared with analytical approximations for low and high frequencies. A collection of results is presented and discussed. Modal wave numbers are traced in the complex plane for varying impedance, showing the usual regular modes and surface waves. A study of a vanishing boundary layer (the Ingard limit) showed that, in contrast to the smoothly converging acoustic modes and downstream running acoustic surface wave, the convergence of the other surface waves is numerically more difficult. Effects of (transverse) turning points and exponential decay are discussed. Especially the occurrence of modes insensitive to the wall impedance is pointed out. Cut-on wave numbers of hard-wall modes are presented as a function of frequency. A strongly nonuniform mean flow gives rise to considerable differences between the modal behavior for low and for high frequencies.

Nomenclature

A, Q, R	=	WKB amplitudes
$\mathcal{A}$	=	arbitrary duct cross section
a	=	reference duct radius, height
$\boldsymbol{a}, a_n$	=	coefficients Galerkin expansion
c_0	=	sound speed (dimensional; dimensionless)
c_∞	=	reference sound speed (dimensional)
$\mathrm{d}\ell$	=	line integration element
$\mathrm{d}S$	=	surface integration element
J	=	total number of Gauss–Legendre points
j	=	index Gauss–Legendre grid
$\mathcal{M}, \mathcal{M}_{\nu l}$	=	$N \times N$ Galerkin matrix
m	=	circumferential mode order
N	=	number of Chebyshev terms
n	=	modal index
$\boldsymbol{n}$	=	normal wall vector (into the wall)
p	=	pressure perturbation; modal function
p_0	=	mean pressure (dimensional)
p_0, p_1	=	small-ω expansion of p
r_1, r_2	=	three-dimensional turning points
T_ν	=	Chebyshev polynomial
t	=	time
(u, v)	=	two-dimensional Cartesian velocity
(u, v, w)	=	three-dimensional cylindrical velocity
u_0	=	mean flow velocity (dimensional; dimensionless)
$\boldsymbol{v}$	=	velocity vector
W	=	$(1 - \mu u_0)/c_0$, scaled Ω
W_0	=	$(1 - \mu_0 u_0)/c_0$
$\boldsymbol{x}$	=	position vector; dummy vector
(x, y)	=	two-dimensional Cartesian coordinates
(x, r, θ)	=	three-dimensional cylindrical coordinates
x_j, w_j	=	Gauss–Legendre points, weights
y_1, y_2	=	two-dimensional turning points
Z	=	wall impedance
γ	=	ratio specific heats; WKB wave number
δ	=	boundary-layer thickness parameter
ζ	=	scaled impedance, ωZ
κ, κ_n	=	modal wavenumber
λ	=	dummy eigenvalue
μ	=	scaled κ, κ is equal to $\omega\mu$
μ_0, μ_1	=	small ω expansion of μ
ν	=	index Galerkin expansion
ρ	=	density perturbation
ρ_0	=	mean density (dimensional)
τ, σ	=	parameters of mean flow families
φ	=	test function
ψ_ν	=	Galerkin expansion basis function
Ω	=	$(\omega - \kappa u_0)/c_0$
ω	=	frequency; Helmholtz number
$\hat{}$	=	denotes modal amplitude, ignored later
$\sim$	=	denotes dimensionless variable, ignored later

I. Introduction

DUCT modes are time-harmonic solutions of the linearized compressible Euler equations in a duct, with the property that they are self-similar in the axial direction. This is possible when the duct and medium are constant in the axial direction. They are interesting in aeroacoustics not only because they form a set of building blocks to construct by linear combination more general solutions, but also because, more importantly, they are simple enough to reveal and understand many aspects of sound propagation in ducts.

For example, the mechanism of cutoff explains that sufficiently far away from any harmonic source or scatterer its sound field consists of only a finite number of modes [1,2]; the rotor-alone noise of a fan, consisting of certain specified frequencies and circumferential mode numbers, only exists when the blade tips rotate (approximately) supersonically [1]; the Tyler–Sofrin selection rule for rotor–stator interaction tells for what combinations of rotor blade and stator vane numbers sound is radiated [3]; both mechanisms may be spoiled by distortion modes due to nonuniformities of the mean flow [4,5], for example, due to upwash; the imaginary parts of the prevailing modal wave numbers constitute a simple measure for the quality of acoustic lining; the indirect determination of a liner's impedance by resolving a measured sound field into its modal spectrum is based on modes [6,7].

In the simplest configuration of a lined duct with a uniform medium without mean flow, modes come in two types: (i) acoustic

Presented as Paper 2019-2594 at the 25th AIAA/CEAS Aeroacoustics Conference, Delft, The Netherlands, May 20–23, 2019; received 24 October 2019; revision received 19 February 2020; accepted for publication 25 March 2020; published online 12 May 2020.

*Associate Professor, Department of Mathematics and Computer Science. Associate Fellow AIAA.

modes and (ii) acoustic surface waves [8,9]. With a mean flow and vanishing boundary layer (slip flow), two other types appear: (iii) upstream and (iv) downstream running hydrodynamic surface waves. If the boundary layer is very thin but not vanishing, again another type of surface wave appears (v) due to the interaction with the boundary layer [10]. Under certain conditions the upstream running hydrodynamic surface wave (iii) is really downstream running and in fact an instability. Brambley [11] showed that in the time domain this is one of many instabilities, some of which are absolute (nonconvective) and (in case of slip flow) of infinite growth rate. This causes the slip flow problem to be really ill-posed and therefore well interpretable only if the problem is recast into some regularized form, for example, by taking the boundary-layer thickness small but nonzero [12]. Although this is a serious problem in time-domain models, and this important insight has solved an almost 50-year-lasting puzzle, we will not deal with it here because we will only consider time-harmonic perturbations of a fixed frequency.

Although modes in a shear flow have been studied since the 1950s [13], it is fair to say that almost all our working knowledge and comprehension of modes is based on the basic configuration of a duct with a uniform mean flow. Interaction with a shear flow (refraction, coupling of acoustic energy with mean flow energy [14]) is hardly covered. It is therefore useful to refine our knowledge of modes by including nonuniform flows.

We will consider here modes in a medium with an isentropic mean flow and sound speed varying in the transverse direction. They constitute a class of simple but nontrivial sound waves in a shear flow and a variable sound speed. For typical two-dimensional (2D) and axisymmetric three-dimensional (3D) configurations, they are governed by what has become known as the 2D and 3D Pridmore-Brown equations. In the following we will present a collection of results obtained by numerical and analytical methods.

II. Problem Description

A. General Case

Consider in a duct of a constant cross section with a medium and boundary conditions independent of the axial position, time-harmonic acoustic perturbations $p, \rho, \boldsymbol{v}$ of plane parallel isentropic inviscid mean flow $p_0, \rho_0, \boldsymbol{v}_0$. This mean flow has a uniformly constant mean pressure $p_0 = \rho_0 c_0^2/\gamma$, but varies in the transverse direction with mean velocity $\boldsymbol{v}_0 = u_0(y,z)\boldsymbol{e}_x$, mean density $\rho_0(y,z)$, and mean sound speed $c_0(y,z)$. The boundary conditions are of impedance type. The ratio of specific heats is denoted[†] by $\gamma = C_p/C_v$.

We are interested in sound fields p, described by self-similar solutions called modes, that retain their shape when traveling down the duct. With the given frequency ω and the usual complex notation, they are of the form

$$p(\boldsymbol{x},t) = \hat{p}(y,z)f(x-Vt) = \hat{p}(y,z)\mathrm{e}^{\mathrm{i}\omega(t-x/V)} = \hat{p}(y,z)\mathrm{e}^{\mathrm{i}\omega t-\mathrm{i}\kappa x} \tag{1}$$

and consist of an exponential function multiplied by a shape function $\hat{p}$. This is an eigenfunction with eigenvalue κ of a Laplace-type operator valid on a duct cross section, and satisfies an equation also known as a preform of the Pridmore-Brown equation [2]:

$$\Omega^2\nabla\cdot\left(\frac{1}{\Omega^2}\nabla\hat{p}\right)+(\Omega^2-\kappa^2)\hat{p}=0, \qquad \text{with } \Omega=\frac{\omega-\kappa u_0}{c_0} \tag{2}$$

The other variables $\hat{u}, \hat{v}, \hat{w}$, and $\hat{\rho}$ can be expressed in $\hat{p}$. See Appendix A.

For the boundary conditions we adopt the Ingard–Myers condition [15,16] at a wall with impedance Z. This Z may vary, but for modes it should be independent of x. The condition assumes a vanishingly thin boundary layer and is given by $\mathrm{i}\omega Z(\hat{\boldsymbol{v}}\cdot\boldsymbol{n}) = \mathrm{i}c_0\Omega\hat{p}$, with a normal unit vector $\boldsymbol{n}$ pointing into the wall. For a mean flow vanishing at the wall, it reduces to the common $Z(\hat{\boldsymbol{v}}\cdot\boldsymbol{n}) = \hat{p}$. In terms of $\hat{p}$ and $\nabla\hat{p}$ the condition is

$$\mathrm{i}\omega Z(\nabla\hat{p}\cdot\boldsymbol{n}) = \rho_0 c_0^2\Omega^2\hat{p} \tag{3}$$

(Note that $\rho_0 c_0^2 = \gamma p_0$ constant.) In the time domain, the Ingard–Myers condition has some fundamental issues [11] and a regularized version should be used. In the frequency domain the problems are mild for acoustic modes. With respect to surface modes [8–10], care is in order when modeling a thin but nonzero boundary layer, because these modes are more sensitive to details of the boundary layer than other modes [17,18].

For later use, we note here that Eq. (2) with Eq. (3) and $Z \neq 0$, valid on a duct cross section $\mathcal{A}$ with boundary $\partial\mathcal{A}$, can be expressed in weak form (multiply by φ/Ω^2 and integrate) by the condition that for any smooth *test* function φ

$$\int_{\partial\mathcal{A}}\frac{\rho_0 c_0^2}{\mathrm{i}\omega Z}\hat{p}\varphi\,\mathrm{d}\ell+\iint_{\mathcal{A}}-\frac{1}{\Omega^2}\nabla\hat{p}\cdot\nabla\varphi+\left(1-\frac{\kappa^2}{\Omega^2}\right)\hat{p}\varphi\,\mathrm{d}S=0 \tag{4}$$

Interestingly, the Ingard–Myers condition fits in very neatly.

Eigenvalue κ corresponds to axial wave number κ, and is probably the most important hallmark of a mode. The modes we are interested in constitute the discrete spectrum of Eq. (2) with (3) given by the infinite and countable set $\{\hat{p}_n, \kappa_n\}$. Because of their self-similarity, modes are relatively easy to study and help the understanding of sound propagation in, and interaction with, the mean flow. From linearity they can be used as a basis (building blocks) to construct more general solutions of the equations. With a uniform mean flow and a uniform sound speed, or no mean flow and arbitrary sound speed, the set of modes is rich enough to represent all solutions ([19] Theorem S.12). This is almost, but not exactly, the case with uniform mean flow, where the factor $\omega - \kappa u_0$ in Eq. (2) may be zero at so-called critical layers for a continuum of values of κ [20], and some solutions cannot be described by discrete modes. Except when all modes are cut off (exponentially decaying in the x direction) and vanishingly small, critical layer contributions are small compared with the rest of the field and can be ignored in most practical situations. Altogether, this makes these modes interesting and useful to study.

B. Two-Dimensional and Axisymmetric 3D Cases

The partial differential Eq. (2) that remains for shape function $\hat{p}(y,z)$ is still difficult to analyze. The two most important simplifications are in 2D, a duct for $0 \leqslant y \leqslant a$ and a mean flow only depending on y, and in 3D, a cylindrical hollow duct $0 \leqslant r \leqslant a$ with an axisymmetric mean flow only depending on r.

In 2D (Fig. 1) with

$$p(\boldsymbol{x},t) = \hat{p}(y)\mathrm{e}^{\mathrm{i}\omega t-\mathrm{i}\kappa x} \tag{5}$$

and $u_0 = u_0(y)$, $c_0 = c_0(y)$, we have (primes denote a derivative to y)

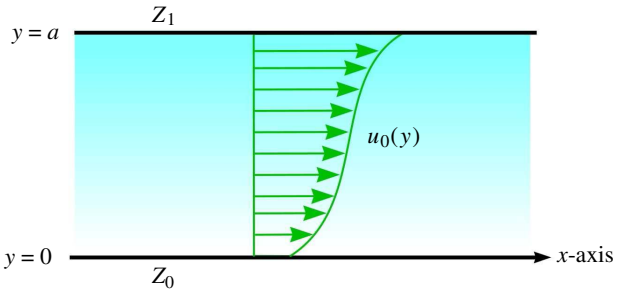

Fig. 1 Two-dimensional configuration with duct of height a, wall impedances Z_0 and Z_1, mean flow $u_0(y)$, and sound speed $c_0(y)$.

[†]Following tradition, we use here γ to denote the ratio of specific heats, but this variable will appear only in the introduction of the problem. Later we will use γ to denote a certain square root. Both notations are not related.

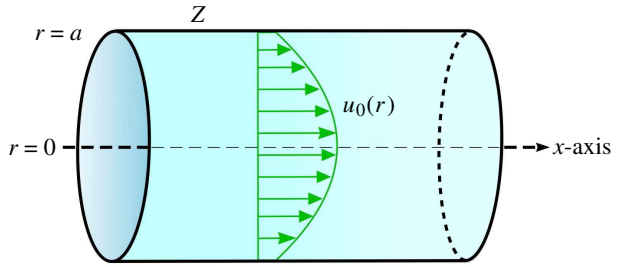

Fig. 2 Three-dimensional axisymmetric configuration with circular duct of radius a, wall impedance Z, mean flow $u_0(r)$, and sound speed $c_0(r)$.

$$\Omega^2\left(\frac{1}{\Omega^2}\hat{p}'\right)' + (\Omega^2-\kappa^2)\hat{p} = 0,$$
$$[\mathrm{i}\omega Z_0\hat{p}' = -\rho_0 c_0^2\Omega^2\hat{p}]_{y=0}, \qquad [\mathrm{i}\omega Z_1\hat{p}' = \rho_0 c_0^2\Omega^2\hat{p}]_{y=a} \tag{6}$$

In an axisymmetric 3D configuration (Fig. 2) with

$$p(\boldsymbol{x},t) = \hat{p}(r)\mathrm{e}^{\mathrm{i}\omega t - \mathrm{i}\kappa x - \mathrm{i}m\theta} \tag{7}$$

where $m \in \mathbb{Z}$ and $u_0 = u_0(r)$, $c_0 = c_0(r)$, we have (primes denote a derivative to r)

$$\frac{\Omega^2}{r}\left(\frac{r}{\Omega^2}\hat{p}'\right)' + \left(\Omega^2-\kappa^2-\frac{m^2}{r^2}\right)\hat{p} = 0,$$
$$[\mathrm{i}\omega Z\hat{p}' = \rho_0 c_0^2\Omega^2\hat{p}]_{r=a}, \qquad p \text{ regular in } r=0 \tag{8}$$

A straightforward generalization would be an annular duct with an impedance condition at the inner wall.

Equations (6) and (8) are, respectively, known as the 2D and 3D Pridmore-Brown equation [2,13]. For a uniform mean flow, Ω is constant and above equations reduce to the standard harmonic equation and the (scaled) Bessel equation, providing analytically exact descriptions of duct modes [1,2,8].

In a nonuniform flow where Ω is a function of y, respectively, r, the Pridmore-Brown equations are in general not solvable in terms of standard functions [13,20–24] and have to be solved numerically. Even in the 2D case of a linear shear flow and a constant sound speed, where an exact solution is known [25] in terms of Weber's parabolic cylinder functions ([26] Chap. 19), the numerical evaluation [27,28] appeared problematic [29] due to the subtraction of exponentially large terms of the constituting parts, and only feasible for a rather limited parameter range. Especially the upstream running modes deteriorate quickly. Numerical solutions are therefore our main source of information. On the other hand, a disadvantage of a numerical solution is the lack of insight that a sufficiently transparent analytical solution provides, possibly (in case of approximations) at the expense of accuracy. Therefore we will discuss both.

Well-known analytical solutions (their origin dating back as far as the early days of quantum mechanics) are Wentzel–Kramers–Brillouin (WKB) approximations[‡] for high values of frequency ω [21]. They provide insight into the (transverse[§]) turning point behavior and give for high-enough ω excellent approximations of modal wave number κ. For general mean flow profiles, this requires a numerical evaluation of integrals that provide the dispersion relation, but for simple mean flows (linear or parabolic profiles) an analytical evaluation is possible.

In the other direction for low frequency (small ω), approximations are also possible, for hard walls and for soft walls. These solutions seem to be not available in the literature, at least not on a systematic basis.

Next to these analytical approaches we will explore a new numerical method based on a Galerkin projection on a Chebyshev basis, with an efficient nonlinear eigenvalue search routine. We will use this method to analyze the behavior of the modes as a function of frequency, impedance, and mean flow profile, with particular interest in surface waves. Furthermore, we will compare the results with the high- and low-frequency approximations.

C. Nondimensional Form

To simplify the equations, and to define exactly what we mean with "ω is small" or "large," it is necessary to have the problems in a nondimensional form. Assuming a characteristic sound speed c_∞, we write

$$y = a\tilde{y}, \quad r = a\tilde{r}, \quad c_0 = c_\infty\tilde{c}_0, \quad u_0 = c_\infty\tilde{u}_0, \quad \hat{p} = \rho_0 c_0^2\tilde{p}$$
$$\omega = \frac{c_\infty}{a}\tilde{\omega}, \quad \Omega = \frac{1}{a}\tilde{\Omega}, \quad \kappa = \frac{1}{a}\tilde{\kappa}, \quad Z = \frac{\rho_0 c_0^2}{c_\infty}\tilde{Z} \tag{9}$$

Dimensionless frequency $\tilde{\omega}$ is also known as the Helmholtz number. Note that $\tilde{Z}$ is not exactly the same as the characteristic impedance $Z/\rho_0 c_0$. It is not really necessary to rescale $\hat{p}$, because any scaling factor drops out the problem, but we added it for consistency. For notational convenience we will further ignore the tildes. Except for $\rho_0 c_0^2 := 1$ and $a := 1$ in the boundary conditions, the equations remain exactly the same, and there is no need to spell out the dimensionless versions.

III. Numerical Solution

Various numerical methods for the Pridmore-Brown equation have been proposed, but they are not equally applicable. Shooting [22] is simple, but only possible if the mode is not vanishingly small near the wall. Collocation methods are more versatile, but sometimes need auxiliary libraries [24] that are not available for MATLAB. Spectral collocation methods applied to the equations in a linearized Euler form, based on or similar to [30], have been favorably used by [31–34].

Therefore, the numerical method chosen here is also a spectral method, but based on a Galerkin projection applied to the 2D and 3D versions[¶] of Eq. (4). The advantage is a compact equation in one variable with $N \times N$ matrices, rather than $4N \times 4N$ in case of Euler equations, if N is the number of basis functions. Especially for the determination of eigenvalues (typically costing $\sim N^3$) this is an important difference. A disadvantage is the fact that the eigenvalue equation is nonlinear, which requires a Newton-type iteration for each eigenvalue. This, however, is not a great problem for our purposes, because we are interested in only the first few modes, whereas the iteration takes usually no more than a single step when tracing for a varying parameter.

An alternative could be multiplying out the Pridmore-Brown equation such that the prevailing matrix eigenvalue problem becomes a third-order polynomial in κ [35], but also this would still be equivalent to a $3N \times 3N$ system.

A. Galerkin Projection

We start with the 2D problem (6) with impedances $Z_{0,1} \neq 0$ in the equivalent form (4) that for *every* test function φ

$$\left.\frac{p\varphi}{\mathrm{i}\omega Z_1}\right|_1 + \left.\frac{p\varphi}{\mathrm{i}\omega Z_0}\right|_0 + \int_0^1 -\frac{1}{\Omega^2}p'\varphi' + \left(1-\frac{\kappa^2}{\Omega^2}\right)p\varphi\,\mathrm{d}y = 0 \tag{10}$$

If we assume that p can be written as a sum over a function basis $\{\psi_\nu\}$,

[‡]The WKB or WKBJ method, named after Gregor Wentzel, Hans Kramers, Leon Brillouin, and Harold Jeffreys, is a multiple-scales-type method to construct asymptotic approximations for waves in a slowly varying medium.

[§]In this paper, only turning point behavior in the transverse direction is considered. Other turning point behaviors may exist in the axial direction, but only if the duct diameter or mean flow varies gradually in the axial direction. In that case, κ turns from real to complex. Strictly speaking, we have then only approximate modes.

[¶]With a suitable basis and quadrature routine, a generalization to the full version of Eq. (4) is straightforward.

$$p = \sum_{\nu=0}^{\infty} a_\nu \psi_\nu \tag{11}$$

and we use the same basis for the test functions, that is, $\varphi = \psi_l$, $l = 0, 1, \ldots$, then Eq. (10) becomes equivalent with

$$\sum_{\nu=0}^{\infty} a_\nu \left[\left. \frac{\psi_\nu \psi_l}{\mathrm{i}\omega Z_1} \right|_1 + \left. \frac{\psi_\nu \psi_l}{\mathrm{i}\omega Z_0} \right|_0 + \int_0^1 \left\{ -\frac{1}{\Omega^2} \psi_\nu' \psi_l' + \left(1 - \frac{\kappa^2}{\Omega^2}\right) \psi_\nu \psi_l \right\} \mathrm{d}y \right] = 0 \tag{12}$$

This can also be written in matrix form

$$\mathcal{M}(\kappa)\boldsymbol{a} = 0, \qquad \boldsymbol{a} = (a_0, a_1, \ldots)^T \tag{13}$$

for the $[0, \infty) \times [0, \infty)$ matrix $\mathcal{M}$ with elements

$$\mathcal{M}_{\nu l}(\kappa) = \left. \frac{\psi_\nu \psi_l}{\mathrm{i}\omega Z_1} \right|_1 + \left. \frac{\psi_\nu \psi_l}{\mathrm{i}\omega Z_0} \right|_0 + \int_0^1 \left\{ -\frac{1}{\Omega^2} \psi_\nu' \psi_l' + \left(1 - \frac{\kappa^2}{\Omega^2}\right) \psi_\nu \psi_l \right\} \mathrm{d}y \tag{14}$$

The nonlinear eigenvalue problem is then approximated by cutting off $\mathcal{M}$ to an $N \times N$ matrix and finding those discrete values of κ, and its corresponding solution space $\boldsymbol{a}$, for which $\mathcal{M}$ has a nonempty null space. Only the first few, absolutely smallest, κ will be of interest as well as numerically accurate.

We choose Chebyshev polynomials on $[0, 1]$

$$\psi_\nu(y) = T_\nu(2y - 1) = \cos(\nu \arccos(2y - 1)) \tag{15}$$

Another option would be to take a Fourier basis (sines and cosines). For the 2D problem this appears to work out equally well. In all the examples we favored Chebyshev polynomials because of their simple generation numerically.

We have a serious problem if $\Omega(y_0) = 0$ for some $y_0 \in [0, 1]$ (a critical layer, as discussed in the Introduction), but this occurs very rarely and apparently not for modes. See [20].

The approach for the 3D problem (8) is similar, with special attention to the singularity at $r = 0$. We can rewrite the equation with the boundary condition ($Z \neq 0$) in the equivalent form (4) that for *every* test function φ

$$\left. \frac{p\varphi}{\mathrm{i}\omega Z} \right|_1 + \int_0^1 \left\{ -\frac{1}{\Omega^2} p'\varphi' + \left(1 - \frac{\kappa^2}{\Omega^2} - \frac{m^2}{r^2\Omega^2}\right) p\varphi \right\} r \, \mathrm{d}r = 0 \tag{16}$$

An important difference with the 2D problem (10) is the singularity in $r = 0$ if $m \neq 0$. Following [36] (see also [37] Sec. 18.5), this has been dealt with by formally extending the solution symmetrically if m is even, and antisymmetrically if m is odd. As a result we know in advance that p can be written as a sum of even basis functions if m is even, and odd basis functions if m is odd. For the same reason we need only even or odd test functions if m is even or odd. This is seen as follows.

If $u_0(r)$ and $c_0(r)$ are smooth in $r = 0$ (physically the only configuration that makes sense) and symmetric in r, it is easily checked by a formal Taylor expansion of $p(r)$ that a regular solution behaves like

$$p(r) = O(r^{|m|}) \quad \text{for } r \to 0 \tag{17}$$

So for a smooth solution it is necessary to extend p symmetrically, that is, $p(r) = p(-r)$, if m is even, and antisymmetrically, that is, $p(r) = -p(-r)$, if m is odd. Now consider the singularity at $r = 0$. If $m = 0$ there is no singularity, and so this case is not a problem. If m is odd $\geqslant 1$ and $\varphi(r) = r\varphi'(0) + \ldots$ antisymmetric, the integrand behaves like

$$\left(-mr^{m-1}\varphi'(0) - \frac{m^2}{r^2} r^m r\varphi'(0)\right) r + \ldots = -m(m+1) r^m \varphi'(0) + \ldots \tag{18}$$

So there is no singularity and the integrand vanishes at $r = 0$. If m is even $\geqslant 2$ and $\varphi(r) = \varphi(0) + r^2\varphi''(0) + \ldots$ symmetric, the integrand behaves like

$$\left(-mr^{m-1} 2r\varphi''(0) - \frac{m^2}{r^2} r^m \varphi(0)\right) r + \ldots = -m^2 r^{m-1} \varphi(0) + \ldots \tag{19}$$

Since $m - 1 \geqslant 1$ there is also here no singularity and the integrand again vanishes.

So there appears to be no singularity at the origin with $p(r)$ itself. That does not immediately guarantee a smooth behavior when p is written as a sum over basis functions, which individually do not have the smooth $O(r^{|m|})$ behavior. Nevertheless, partly because the Gauss–Legendre nodes (see below) do not include the origin, there were never problems and the convergence was smooth and fast.

Again we choose a basis of Chebyshev polynomials, but now on $[-1, 1]$. So

$$\psi_\nu(r) = \begin{cases} T_{2\nu}(r) = \cos(2\nu \arccos r) & \text{if } m \text{ is even,} \\ T_{2\nu+1}(r) = \cos((2\nu+1) \arccos r) & \text{if } m \text{ is odd} \end{cases} \tag{20}$$

A Fourier basis is also possible, but comparison with exact solutions in a uniform flow suggests that results with Chebyshev bases are slightly smoother.

While taking the above into consideration, we assume that p can be written as a sum over this function basis $\{\psi_\nu\}$,

$$p = \sum_{\nu=0}^{\infty} a_\nu \psi_\nu \tag{21}$$

Equation (16) becomes equivalent (with $\varphi = \psi_l$, and $l = 0, 1, \ldots$) with

$$\sum_{\nu=0}^{\infty} a_\nu \left[\left. \frac{\psi_\nu \psi_l}{\mathrm{i}\omega Z} \right|_1 + \int_0^1 \left\{ -\frac{1}{\Omega^2} \psi_\nu' \psi_l' + \left(1 - \frac{\kappa^2}{\Omega^2} - \frac{m^2}{r^2\Omega^2}\right) \psi_\nu \psi_l \right\} r \, \mathrm{d}r \right] = 0 \tag{22}$$

This can also be written in matrix form

$$\mathcal{M}(\kappa)\boldsymbol{a} = 0, \qquad \boldsymbol{a} = (a_0, a_1, \ldots)^T \tag{23}$$

for the $[0, \infty) \times [0, \infty)$ matrix $\mathcal{M}$ with elements

$$\mathcal{M}_{\nu l}(\kappa) = \left. \frac{\psi_\nu \psi_l}{\mathrm{i}\omega Z} \right|_1 + \int_0^1 \left\{ -\frac{1}{\Omega^2} \psi_\nu' \psi_l' + \left(1 - \frac{\kappa^2}{\Omega^2} - \frac{m^2}{r^2\Omega^2}\right) \psi_\nu \psi_l \right\} r \, \mathrm{d}r \tag{24}$$

Again, for the nonlinear eigenvalue problem we cut off $\mathcal{M}$ to an $N \times N$ matrix and find those discrete values of κ for which $\mathcal{M}$ has a nonempty null space and corresponding solution space $\boldsymbol{a}$.

B. Special Case of $Z = 0$

The problem with boundary conditions corresponding to a pressure release wall ($Z = 0$) cannot be formulated in a weak form like above. So any Galerkin procedure has to follow another strategy. The usual route is to use the fact that we may expect uniform convergence, and so, if we choose a basis that vanishes at the interval ends, also their sum will vanish there. This can be understood as follows.

If we consider the weak formulation with *natural* boundary conditions (Eq. (10) or (16) for hard walls), then it is common for this type of problems (standard theory [37] (Chap. 3), [38] (Chap. 1), [39]

(Chap. 2) cannot be applied directly) that the Galerkin projection converges in a Sobolev space H^1, which means both the function and its derivative. This implies for one-dimensional problems uniform convergence. So by choosing a basis that vanishes at one or both ends of the interval (spanning a Sobolev space H_0^1, a subspace of H^1) we have guaranteed a solution that also vanishes at the boundary or boundaries.

For this problem it is not convenient to choose a Chebyshev basis because Chebyshev polynomials do not vanish at the interval ends, but a Fourier basis of the right type works well.

C. Nonlinear Eigenvalue Problem

Because the eigenvalue problem (Eq. (13) or (23)) is nonlinear, its numerical solution is not straightforward. For example, to find numerically the zeros of $\det(\mathcal{M}(\kappa))$ is a very unstable process for matrices larger than (say) 20×20 and therefore not an option. A number of approaches, working on the matrix itself, have been reviewed in [35]. In here, Algorithm 3, "Method of successive linear problems", is both simple to implement and efficient in operation (under normal conditions quadratically convergent). Because we mainly study the problem parameter dependence of the first few modes, and trace the eigenvalue in small steps such that each step gives an excellent starting value for the next one, the iteration is no limitation given the other advantages, and the method appeared indeed suitable for our purposes. The method is in structure similar to Newton's method, and runs as follows.

Let a starting value $\kappa = \kappa_0$ be given. The corresponding vector $\boldsymbol{a}_0$ is not important. Finding a good starting value is a problem on its own, but tracking with small steps in u_0 and Z from a known configuration (uniform flow, hard walls), or a preparatory zeroth step with a reasonably dense distribution of starting values in the range of interest, works well.

Suppose that we have the jth iterated eigenvalue approximation κ_j with amplitude vector $\boldsymbol{a}_j$. Linearize for κ near κ_j

$$\mathcal{M}(\kappa) = \mathcal{M}(\kappa_j) + (\kappa - \kappa_j)\mathcal{M}'(\kappa_j) + \ldots \tag{25}$$

Assuming a convergent process, we construct the $j+1$ st iterated eigenvalue κ_{j+1} with vector $\boldsymbol{a}_{j+1}$ by solving the approximate equation

$$\mathcal{M}(\kappa_{j+1})\boldsymbol{a}_{j+1} \simeq \{\mathcal{M}(\kappa_j) + (\kappa_{j+1} - \kappa_j)\mathcal{M}'(\kappa_j)\}\boldsymbol{a}_{j+1} = 0 \tag{26}$$

This can be done by standard methods for solving the generalized eigenvalue problem

$$\mathcal{M}(\kappa_j)\boldsymbol{x} = \lambda\mathcal{M}'(\kappa_j)\boldsymbol{x} \tag{27}$$

with solutions $\lambda_1, \lambda_2, \ldots$ and $\boldsymbol{x}_1, \boldsymbol{x}_2, \ldots$. Choose from all λ's the absolutely smallest, $\lambda_{\min}$, and identify $\kappa_{j+1} = \kappa_j - \lambda_{\min}$ and $\boldsymbol{a}_{j+1} = \boldsymbol{x}$, where $\boldsymbol{x}$ corresponds to this $\lambda_{\min}$. Iterate until $\|\mathcal{M}(\kappa_j)\boldsymbol{a}_j\|$ is small enough. This simple and elegant iteration converges quadratically.

The derivatives $\mathcal{M}'$ are easily obtained analytically. For the 2D case (14) it is

$$\mathcal{M}'_{\nu l}(\kappa) = -2\int_0^1 \frac{1}{c_0\Omega^3}\{u_0\psi'_\nu\psi'_l + \kappa\omega\psi_\nu\psi_l\}\,\mathrm{d}y \tag{28}$$

For the 3D case (24) it is

$$\mathcal{M}'_{\nu l}(\kappa) = -2\int_0^1 \frac{r}{c_0\Omega^3}\left\{u_0\psi'_\nu\psi'_l + \left(\kappa\omega + \frac{m^2}{r^2}u_0\right)\psi_\nu\psi_l\right\}\mathrm{d}r \tag{29}$$

The $\mathcal{M}_{\nu l}$ and $\mathcal{M}'_{\nu l}$ integrals are determined numerically by the efficient Gauss–Legendre integration rule, which amounts to an approximation of the form

$$\int_a^b f(x)\,\mathrm{d}x \simeq \sum_{j=0}^{J} w_j f(x_j) \tag{30}$$

with nodes x_j and weights w_j chosen such that all polynomials of degree $2J+1$ and less are evaluated exactly. The method appears to be very accurate already for a moderate number of nodes (typically between 20 and 60, but at least a little above N), except when the resolution of steep variations of the mean flow asks for a finer grid and more basis functions.

The number of terms of the series over basis ψ_ν is typically $N = 20$ or 40. Lower values ($N = 5$ or $N = 10$) are sometimes sufficient (when the mode shape has no nodes or exponentially small parts), but for high-cutoff modes, certain surface waves, higher frequencies, and sharp changes in the mean flow like thin boundary layers, higher values of N and J may become necessary. It goes without saying that with plots for varying parameter values no risk was taken and a wide margin was kept.

To assess the accuracy and convergence rates, comparisons with exact solutions with constant u_0 and c_0 were carried out (Table 1). Similar tests for other mean flow profiles show the same trends. They confirm exponential convergence in N (common for spectral methods), and a quadratic convergence of the iteration. Normally within a few iteration steps full convergence (a little above machine accuracy) is achieved.

The typical calculation time (including the generation of the basis functions, the matrices, and all iterations) is in the order of 0.05 s (MATLAB 2018, Intel Core i5-4670 CPU@3.4 GHz), which is about

Table 1 Convergence test with analytically exact solution in 2D (a, b) and 3D (c, d)

a) Convergence of iteration (0.058 s)		
$\kappa_{\mathrm{ex}} = -25.467933059613 + 0.952279738435\mathrm{i}$		
$\kappa_0 = -25.0 + 0.0\mathrm{i}, N = 24, J = 25$		
n	κ_n	$\lvert\kappa_n - \kappa_{n-1}\rvert$
1	$-25.463084906355 + 0.961257265835\mathrm{i}$	1.066987891971
2	$-25.467932374742 + 0.952279163171\mathrm{i}$	0.010203150357
3	$-25.467933059613 + 0.952279738435\mathrm{i}$	0.000000894414
b) Convergence in N (with minimum J)		
N	J	$\lvert\kappa_N - \kappa_{\mathrm{ex}}\rvert$
16	17	3.24E − 05
18	19	2.79E − 07
20	21	1.48E − 09
22	23	5.10E − 12
24	25	3.22E − 14
c) Convergence of iteration (0.037 s)		
$\kappa_{\mathrm{ex}} = -13.869291717445 + 8.302294924552\mathrm{i}$		
$\kappa_0 = -13.0 + 8.0\mathrm{i}, N = 14, J = 21$		
n	κ_n	$\lvert\kappa_n - \kappa_{n-1}\rvert$
1	$-13.877049699080 + 8.249630478535\mathrm{i}$	0.911883518038
2	$-13.869314923640 + 8.302464292787\mathrm{i}$	0.053396991296
3	$-13.869291718400 + 8.302294925913\mathrm{i}$	0.000170949177
d) Convergence in N (with minimum J)		
N	J	$\lvert\kappa_N - \kappa_{\mathrm{ex}}\rvert$
6	9	2.96E − 2
8	11	9.88E − 4
10	15	1.50E − 5
12	18	1.01E − 7
14	21	1.66E − 9

Iteration converges (better than) quadratically; the convergence in N exponentially $\sim 10^{-N}$. $c_0 = 1$, $u_0 = 0.5$. (a, b) $\omega = 20$, $Z_0 = Z_1 = 1 + 2\mathrm{i}$; (c, d) $\omega = 20$, $m = 20$, $Z = 1 + 2\mathrm{i}$.

10–20 times faster than the solution of the exact eigenvalue equation by MATLAB's fsolve.

Other nontrivial, useful checks were the various exact integrals given in Appendix B.

IV. Asymptotic Solution for ω Small

In 2D, and 3D with $m = 0$, and hard walls, there is for $\omega = 0$ a real eigenvalue $\kappa = 0$ and infinitely many imaginary. We consider here the neighborhood of $\kappa = 0$ in the limit of small ω. By scaling and balancing terms in the differential equations, it is quickly found that eigenvalue $\kappa = O(\omega)$. Therefore, we rescale $\kappa = \omega\mu$, $\Omega = \omega(1 - \mu u_0)/c_0 = \omega W$.

A. Two-Dimensional and Hard Walls

We have for 2D

$$\left(\frac{1}{W^2}p'\right)' + \omega^2\left(1 - \frac{\mu^2}{W^2}\right)p = 0 \tag{31}$$

with $p'(0) = p'(1) = 0$, and p and μ to be found. We expand in powers of ω^2

$$p = p_0 + \omega^2 p_1 + \omega^4 p_2 + \ldots, \qquad \mu = \mu_0 + \omega^2\mu_1 + \ldots \tag{32}$$

After collecting equal orders of magnitude, and introducing $W_0 = (1 - \mu_0 u_0)/c_0$, we find to leading orders

$$(W_0^{-2}p_0')' = 0,$$
$$(W_0^{-2}p_1')' = -2(\mu_1 u_0 c_0^{-1} W_0^{-3} p_0')' - (1 - \mu_0^2 W_0^{-2})p_0$$

and boundary conditions $p_0' = p_1' = 0$ at $y = 0$ and $y = 1$. It immediately follows that $p_0' = 0$ and so $p_0 = 1$ (or any other constant, but this is unimportant for an eigensolution). As a result we find for the next order

$$p_1' = W_0^2\left[-y + \mu_0^2\int_0^y W_0^{-2}\,\mathrm{d}y'\right] \tag{33}$$

The boundary condition at $y = 1$ yields an algebraic equation for μ_0, valid for any u_0 and c_0:

$$\mu_0^2\int_0^1 W_0^{-2}\,\mathrm{d}y' = \mu_0^2\int_0^1 \frac{c_0^2}{(1 - \mu_0 u_0)^2}\,\mathrm{d}y' = 1 \tag{34}$$

This is a general result, but finding μ_0 requires numerical evaluation. For a linear flow profile and a constant sound speed

$$u_0 = \tau + \sigma y, \qquad c_0 = 1 \tag{35}$$

the analysis can be performed analytically exactly. We have

$$\int \frac{1}{(1 - \mu_0 u_0)^2}\,\mathrm{d}y = \frac{1}{\mu_0\sigma(1 - \mu_0 u_0)} \tag{36}$$

provided $1 - \mu_0 u_0 \neq 0$ for $0 \leqslant y \leqslant 1$, which is indeed confirmed by the final result

$$\mu_0^{\pm} = \frac{\pm 1}{\sqrt{1 + \frac{1}{4}\sigma^2} \pm (\tau + \frac{1}{2}\sigma)} \tag{37}$$

The corresponding wave numbers and eigenfunctions with normalization $p(0) = 1$ are

$$\kappa^{\pm} = \frac{\pm\omega}{\sqrt{1 + \frac{1}{4}\sigma^2} \pm (\tau + \frac{1}{2}\sigma)} + O(\omega^3) \tag{38a}$$

$$p^{\pm} = 1 - \omega^2\mu_0^{\pm}\sigma y^2\left[(1 - \mu_0^{\pm}\tau)\left(\tfrac{1}{2} - \tfrac{1}{3}y\right) - \mu_0^{\pm}\sigma\left(\tfrac{1}{3}y - \tfrac{1}{4}y^2\right)\right] + O(\omega^4) \tag{38b}$$

This result is exact for a uniform profile where $\sigma = 0$.

B. Two-Dimensional and Impedance Walls

For impedance conditions the asymptotics depend on the order of magnitude of $Z_{0,1}$ in terms of a small parameter ω. There are many possible limits and we will not consider them all, but just a few that seem the more interesting ones. With again $\kappa = \omega\mu$ we see from the boundary condition

$$\mathrm{i}\omega Z p' = \pm\omega^2 W^2 p \tag{39}$$

that any impedance $Z \gg O(\omega)$ yields a perturbation of hard wall conditions. In order not to mix up the expansion (32) in powers of ω^2 suggested by Eq. (31), we choose[**] $Z_{0,1} = O(\omega^{-1})$ and rescale

$$\omega Z_0 = \zeta_0, \qquad \omega Z_1 = \zeta_1 \tag{40}$$

with $\zeta_{0,1} = O(1)$ and consider the boundary conditions

$$\mathrm{i}\zeta_0 p' = -\omega^2 W^2 p \text{ at } y = 0, \qquad \mathrm{i}\zeta_1 p' = \omega^2 W^2 p \text{ at } y = 1 \tag{41}$$

Expansion of p results to leading order $p_0 = 1$. Higher orders can in principle be found for any profiles, but for the linear profile (35) we find analytically exactly

$$\kappa^{\pm} = \frac{\pm\omega}{\sqrt{1/(1 - \mathrm{i}(\zeta_0^{-1} + \zeta_1^{-1})) + \frac{1}{4}\sigma^2} \pm (\tau + \frac{1}{2}\sigma)} + O(\omega^3) \tag{42a}$$

with eigensolutions $p = p_0 + \omega^2 p_1 + \ldots$ (normalized by $p(0) = 1$), where

$$p_1^{\pm}(y) = \mathrm{i}\zeta_0^{-1} y\left(\tfrac{1}{3}(y\mu_0^{\pm}\sigma)^2 - y\mu_0^{\pm}\sigma(1 - \mu_0^{\pm}\tau) + (1 - \mu_0^{\pm}\tau)^2\right)$$
$$- y^2\left(\tfrac{1}{4}(y\mu_0^{\pm}\sigma)^2 - \tfrac{1}{3}y\mu_0^{\pm}\sigma\left(2(1 - \mu_0^{\pm}\tau) - \frac{\mu_0^{\pm 2}}{1 - \mu_0^{\pm}\tau}\right)\right.$$
$$\left. + \tfrac{1}{2}((1 - \mu_0^{\pm}\tau)^2 - \mu_0^{\pm 2})\right) \tag{42b}$$

This approximation remains valid if one or both sides are hard. In that case simply $\zeta_0^{-1} = 0$ or $\zeta_1^{-1} = 0$. If Z_0 or Z_1 are zero, we need a separate analysis. For example, if $Z_0 = Z_1 = 0$, we find to leading order

$$\kappa^{\pm} = \frac{\omega}{\tau + \frac{1}{2}(1 \pm \mathrm{i}\sqrt{3})\sigma} + O(\omega^3) \tag{43a}$$

with (arbitrarily normalized) eigensolution

$$p_0^{\pm} = y(1 - y)\left(y - \tfrac{1}{2} \mp \mathrm{i}\tfrac{1}{2}\sqrt{3}\right) \tag{43b}$$

C. Three-Dimensional and Hard Walls

For the 3D, $m = 0$, problem we can follow a similar strategy to find

$$\left(\frac{r}{W^2}p'\right)' + \omega^2 r\left(1 - \frac{\mu^2}{W^2}\right)p = 0 \tag{44}$$

leading to

[**]Other scalings can be analyzed on a case-by-case basis.

$$(rW_0^{-2}p_0')' = 0,$$
$$(rW_0^{-2}p_1')' = -2(r\mu_1 u_0 c_0^{-1} W_0^{-3} p_0')' - r(1-\mu_0^2 W_0^{-2})p_0$$

For hard walls with $p_0'(1) = 0$ it follows that $p_0 = 1$. Then

$$p_1' = -\frac{1}{2} rW_0^2 + \mu_0^2 \frac{W_0^2}{r} \int_0^r \frac{r'}{W_0^2}\, \mathrm{d}r' \tag{45}$$

$p_1'(1) = 0$ yields (ignoring the singular solution $1 - \mu_0 u_0(1) = 0$) the algebraic equation for μ_0

$$\mu_0^2 \int_0^1 \frac{r'}{W_0^2}\, \mathrm{d}r' = \mu_0^2 \int_0^1 \frac{r' c_0^2}{(1-\mu_0 u_0)^2}\, \mathrm{d}r' = \frac{1}{2} \tag{46}$$

This is again a general result, valid for any (physical) profiles u_0 and c_0, but finding μ_0 requires numerical evaluation. For parabolic profiles

$$u_0 = \tau - \sigma r^2, \qquad c_0 = 1 \tag{47}$$

we can derive analytically exact results by using

$$\int \frac{r}{(1-\mu_0 u_0)^2}\, \mathrm{d}r = -\frac{1}{2\mu_0 \sigma (1-\mu_0 u_0)} \tag{48}$$

provided $\mu_0 u_0 \neq 1$ for $0 \leqslant r \leqslant 1$. This is indeed satisfied by the resulting modal wave numbers

$$\kappa^{\pm} = \frac{\pm\omega}{\sqrt{1 + \frac{1}{4}\sigma^2} \pm (\tau - \frac{1}{2}\sigma)} + O(\omega^3) \tag{49a}$$

(This result is exact for a uniform profile where $\sigma = 0$.) The derivative p_1' is

$$p_1' = \frac{1}{2}\sigma \frac{\tau(1-\mu_0^{\pm}\tau) - \mu_0^{\pm}}{(1-\mu_0^{\pm}\tau)(\tau^2 - \sigma\tau - 1)} r(1-r^2)(1-\mu_0^{\pm} u_0(r))$$

and so, with normalization $p(0) = 1$, the corresponding eigensolutions are

$$p^{\pm} = 1 + \frac{1}{4}\omega^2 \sigma \frac{\tau(1-\mu_0^{\pm}\tau) - \mu_0^{\pm}}{(1-\mu_0^{\pm}\tau)(\tau^2 - \sigma\tau - 1)} \cdots$$
$$\times r^2 \Big[(1-\mu_0^{\pm}\tau)\big(1 - \tfrac{1}{2}r^2\big) - \mu_0^{\pm}\sigma\big(1 - r^2 + \tfrac{1}{3}r^4\big) \Big] + O(\omega^4) \tag{49b}$$

D. Three-Dimensional and Impedance Walls

The effect of the regularity condition at the origin is that the leading order solution p_0 can only be a constant if ω is small and $\kappa = O(\omega)$. So for a manageable and interesting problem we rescale

$$\omega Z = \zeta \tag{50}$$

with $\zeta = O(1)$, leading for the parabolic mean flow profile (47) to the boundary condition

$$\mathrm{i}\zeta p_1' = (1 - \mu_0(\tau - \sigma))^2 \quad \text{at } r = 1 \tag{51}$$

By using Eqs. (45) and (48) we arrive at the algebraic equation for μ_0

$$\frac{1}{2}\mathrm{i}\zeta(1-\mu_0(\tau-\sigma))\left(\frac{\mu_0^2}{1-\mu_0\tau} - 1 + \mu_0(\tau-\sigma)\right) = (1-\mu_0(\tau-\sigma))^2$$

with eventually the solutions

$$\kappa^{\pm} = \frac{\pm\omega}{\sqrt{(1/(1-2\mathrm{i}\zeta^{-1})) + \frac{1}{4}\sigma^2} \pm (\tau - \frac{1}{2}\sigma)} + O(\omega^3) \tag{52}$$

and a hydrodynamic mode $\kappa \simeq \omega\mu_0 = \omega/(\tau - \sigma)$ (to leading order no pressure, only velocity components). The corresponding eigensolutions can be constructed by integration of p_1'.

If $Z = 0$ we need a separate analysis. It transpires that κ remains $O(1)$ for $\omega \to 0$ (in particular its imaginary part), and the equation for p does not simplify unless u_0 and c_0 are constant. As a result there is no simple analytical approximation of the present type.

E. Duct of General Cross Section

For completeness we give here briefly the analogous results for a 3D duct of general cross section $\mathcal{A}$ and impedance boundary condition along the circumference $\partial\mathcal{A}$. Because the (now dimensionless) prevailing equation (2) remains essentially a partial differential equation, there are little possibilities to obtain an explicit expression for the modal shape function, but for the wave number an equation like above is possible.

With the same scaling as above we have for $(y, z) \in \mathcal{A}$

$$\nabla \cdot \left(\frac{1}{W^2}\nabla p\right) + \omega^2 \left(1 - \frac{\mu^2}{W^2}\right) p = 0 \tag{53}$$

and a (scaled) impedance condition along $\partial\mathcal{A}$

$$\mathrm{i}\zeta \nabla p \cdot \boldsymbol{n} = \omega^2 W^2 p \tag{54}$$

We expand $p = p_0 + \omega^2 p_1 + \ldots, \mu = \mu_0 + \omega^2 \mu_1 + \ldots$ and find to leading order

$$\nabla \cdot \left(\frac{1}{W_0^2}\nabla p_0\right) = 0 \text{ in } \mathcal{A}, \quad \nabla p_0 \cdot \boldsymbol{n} = 0 \text{ along } \partial\mathcal{A} \tag{55}$$

By multiplying by p_0^*, integrating over $\mathcal{A}$, and utilizing Gauss's theorem we find that

$$\begin{aligned} \iint_{\mathcal{A}} p_0^* \nabla \cdot \left(\frac{1}{W_0^2}\nabla p_0\right) \mathrm{d}S &= \iint_{\mathcal{A}} \nabla \cdot \left(\frac{p_0^*}{W_0^2}\nabla p_0\right) - \frac{1}{W_0^2}|\nabla p_0|^2\, \mathrm{d}S \\ &= \int_{\partial\mathcal{A}} \frac{p_0^*}{W_0^2}\nabla p_0 \cdot \boldsymbol{n}\, \mathrm{d}\ell - \iint_{\mathcal{A}} \frac{1}{W_0^2}|\nabla p_0|^2\, \mathrm{d}S \\ &= -\iint_{\mathcal{A}} \frac{1}{W_0^2}|\nabla p_0|^2\, \mathrm{d}S = 0 \end{aligned} \tag{56}$$

Because the integral of a nonnegative function can only vanish if the function is identically zero, we have $|\nabla p_0| = 0$, and therefore $p_0 = 1$, that is, a constant, which can be taken equal to unity.

The equation for p_1 is then

$$\nabla \cdot \left(\frac{1}{W_0^2}\nabla p_1\right) = -1 + \frac{\mu_0^2}{W_0^2} \text{ in } \mathcal{A}, \qquad \mathrm{i}\zeta \nabla p_1 \cdot \boldsymbol{n} = W_0^2 \text{ along } \partial\mathcal{A} \tag{57}$$

After integration along $\mathcal{A}$, applying Gauss's theorem and the boundary condition, we find

$$\begin{aligned} \iint_{\mathcal{A}} \nabla \cdot \left(\frac{1}{W_0^2}\nabla p_1\right) \mathrm{d}S &= \int_{\partial\mathcal{A}} \frac{1}{W_0^2}\nabla p_1 \cdot \boldsymbol{n}\, \mathrm{d}\ell \\ &= \int_{\partial\mathcal{A}} \frac{1}{\mathrm{i}\zeta}\, \mathrm{d}\ell = -\iint_{\mathcal{A}} \left(1 - \frac{\mu_0^2}{W_0^2}\right) \mathrm{d}S \end{aligned} \tag{58}$$

And so (leaving the possibility open that ζ varies along $\partial\mathcal{A}$) we have the equation that determines μ_0

$$\int_{\partial\mathcal{A}} \frac{1}{\mathrm{i}\zeta}\,\mathrm{d}\ell + |\mathcal{A}| - \mu_0^2 \iint_{\mathcal{A}} \frac{1}{W_0^2}\,\mathrm{d}S = 0 \tag{59}$$

where $|\mathcal{A}|$ denotes the size of surface $\mathcal{A}$. The hard-wall case is included by taking $1/\zeta = 0$. Equation (59) has to be solved numerically, except possibly for very simple mean flow profiles, like a constant u_0 and c_0. Then we find

$$\kappa^{\pm} = \frac{\pm\omega\eta}{c_0 \pm \eta u_0} + O(\omega^3), \qquad \eta = \left(1 + \frac{1}{|\mathcal{A}|}\int_{\partial\mathcal{A}} \frac{1}{\mathrm{i}\zeta}\mathrm{d}\ell\right)^{\frac{1}{2}} \tag{60}$$

V. WKB Solution for ω Large

The used WKB solution [40] (Chap. 10), [41] (Sec. 15.4.2) is comparable to what has been studied in [21], and so we will just give a concise derivation. We will only consider the hard wall case. Soft walls can be included, but the evaluation is very laborious while the shielding of an impedance wall by a turning point (see below) is best understood with hard walls.

A. Two-Dimensional and Hard Walls

Consider

$$\Omega^2\left(\frac{1}{\Omega^2}p'\right)' + (\Omega^2 - \kappa^2)p = 0, \qquad p'(0) = p'(1) = 0 \tag{61}$$

for large ω. We postulate cut-on modes for real κ not near resonance, that is, $\kappa = O(\omega)$ and $\Omega = O(\omega)$. We make the WKB–Ansatz (with phase function $\gamma = O(\omega)$ to be determined)

$$p(y) = A(y)\mathrm{e}^{-\mathrm{i}\int^y \gamma(z)\,\mathrm{d}z} \tag{62}$$

such that

$$(-\gamma^2 + \Omega^2 - \kappa^2)A - \frac{\mathrm{i}\Omega^2}{A}\left(\frac{\gamma A^2}{\Omega^2}\right)' + \Omega^2\left(\frac{A'}{\Omega^2}\right)' = 0 \tag{63}$$

We find to leading order $O(\omega^2)$

$$(-\gamma^2 + \Omega^2 - \kappa^2)A = 0 \tag{64}$$

or (with a suitably chosen sign)

$$\gamma = \sqrt{\Omega^2 - \kappa^2} \tag{65}$$

With this γ, we have then to next order $O(\omega)$

$$\left(\frac{\gamma A^2}{\Omega^2}\right)' = 0 \tag{66}$$

or (with Q a constant)

$$A = Q\frac{\Omega}{\sqrt{\gamma}} = Q\frac{\Omega}{(\Omega^2 - \kappa^2)^{\frac{1}{4}}} \tag{67}$$

We consider first the case of γ real everywhere (i.e., $\gamma^2 > 0$). Then we have along the whole interval the solution

$$p = \frac{\Omega}{(\Omega^2 - \kappa^2)^{\frac{1}{4}}}\left(Q\mathrm{e}^{-\mathrm{i}\int_0^y \gamma\,\mathrm{d}z} + R\mathrm{e}^{\mathrm{i}\int_0^y \gamma\,\mathrm{d}z}\right) \tag{68}$$

To leading order this is at $y = 0$

$$p'(0) \simeq -\mathrm{i}\Omega\sqrt{\gamma}(Q - R) = 0$$

such that $R = Q$. Without loss of generality we can write

Table 2 Comparison of 18 cut-on hard-wall modes

	Numerical	WKB		
n	κ_n	κ_n	y_1	y_2
	a) $[0, y_2]$			
1	+12.7404	+12.7203		0.2410
2	+11.6482	+11.6186		0.7379
	b) $[0, 1]$			
3	+10.9908	+11.0352		
4	+9.7991	+9.8030		
5	+7.9130	+7.9130		
6	+5.2757	+5.2755		
7	+1.6580	+1.6579		
8	−3.4857	−3.4858		
9	−12.2566	−12.2572		
−9	−31.6342	−31.6756		
−8	−39.1405	−39.4023		
	c) $[y_1, 1]$			
−1	−91.7189	−91.0914	0.9348	
−2	−75.6769	−75.6259	0.7851	
−3	−65.7266	−65.7160	0.6522	
−4	−58.1112	−58.1116	0.5194	
−5	−51.9320	−51.9366	0.3830	
−6	−46.7717	−46.7752	0.2414	
−7	−42.5897	−42.3839	0.0937	

WKB approximation and numerical solution ($N = 40$, $J = 80$); 2D duct; $\omega = 20$; linear mean flow profile $u_0 = 0.5 + 0.3y$ and $c_0 = 1$; turning points at y_1 and y_2.

$$p \simeq \frac{\Omega}{\sqrt{\gamma}}\cos\left(\int_0^y \gamma\,\mathrm{d}z\right), \qquad p' \simeq -\Omega\sqrt{\gamma}\sin\left(\int_0^y \gamma\,\mathrm{d}z\right) \tag{69}$$

and we retain at $y = 1$

$$p'(1) \sim \sqrt{\gamma}\sin\left(\int_0^1 \gamma\,\mathrm{d}y\right) = 0 \tag{70}$$

In other words, the (approximate) condition to find eigenvalue κ is

$$\int_0^1 \gamma\,\mathrm{d}y = n\pi, \qquad n \in \mathbb{N} \tag{71}$$

Note that to respect the asymptotics of $\omega \to \infty$ and $\gamma = O(\omega)$, this equation is only valid for sufficiently large n, such that $\omega \sim n\pi$. Usually, however, WKB is very forgiving.

In general this equation is to be solved numerically, even if the mean flow profile is linear, that is, $u_0(y) = \tau + \sigma y$ and $c_0(y) = 1$, and the integral can be found analytically exactly.

Interesting special cases are those with turning points, that is, with γ^2 changing sign along the interval $[0, 1]$. There where γ is imaginary, the wave becomes exponentially small and (apart from a small region beyond the turning point) is practically not present. Consider for convenience the situation of a single turning point $y_1 \in (0, 1)$ with γ real for $y > y_1$. Then we have, taking into account a small region beyond the turning point,[††] the condition

$$\int_{y_1}^1 \gamma\,\mathrm{d}y = \left(n + \frac{1}{4}\right)\pi, \qquad n \in \mathbb{N} \tag{72}$$

Note that this implies that the boundary condition at $y = 0$ plays no role, and so the solution is (asymptotically) the same for any other boundary condition. In this sense, any effect of an impedance wall at $y = 0$ is shielded by the turning point. In the same way, a turning point $y_2 \in (0, 1)$ with γ real for $y < y_2$ gives the condition

[††]This is a result of matching between outer solutions at either side of the turning point and an inner solution in the neighborhood of the turning point [41].

$$\int_0^{y_2} \gamma \,\mathrm{d}y = \left(n + \frac{1}{4}\right)\pi, \qquad n \in \mathbb{N} \tag{73}$$

and makes any boundary condition at $y = 1$ ineffective. Two turning points, $0 < y_1 < y_2 < 1$, with γ real along $[y_1, y_2]$, give

$$\int_{y_1}^{y_2} \gamma \,\mathrm{d}y = \left(n + \frac{1}{2}\right)\pi, \qquad n \in \mathbb{N} \tag{74}$$

and make the solution independent of boundary conditions at both sides.

B. Three-Dimensional and Hard Walls

Consider

$$\frac{\Omega^2}{r}\left(\frac{r}{\Omega^2}\,p'\right)' + \left(\Omega^2 - \kappa^2 - \frac{m^2}{r^2}\right)p = 0, \qquad p'(1) = 0 \tag{75}$$

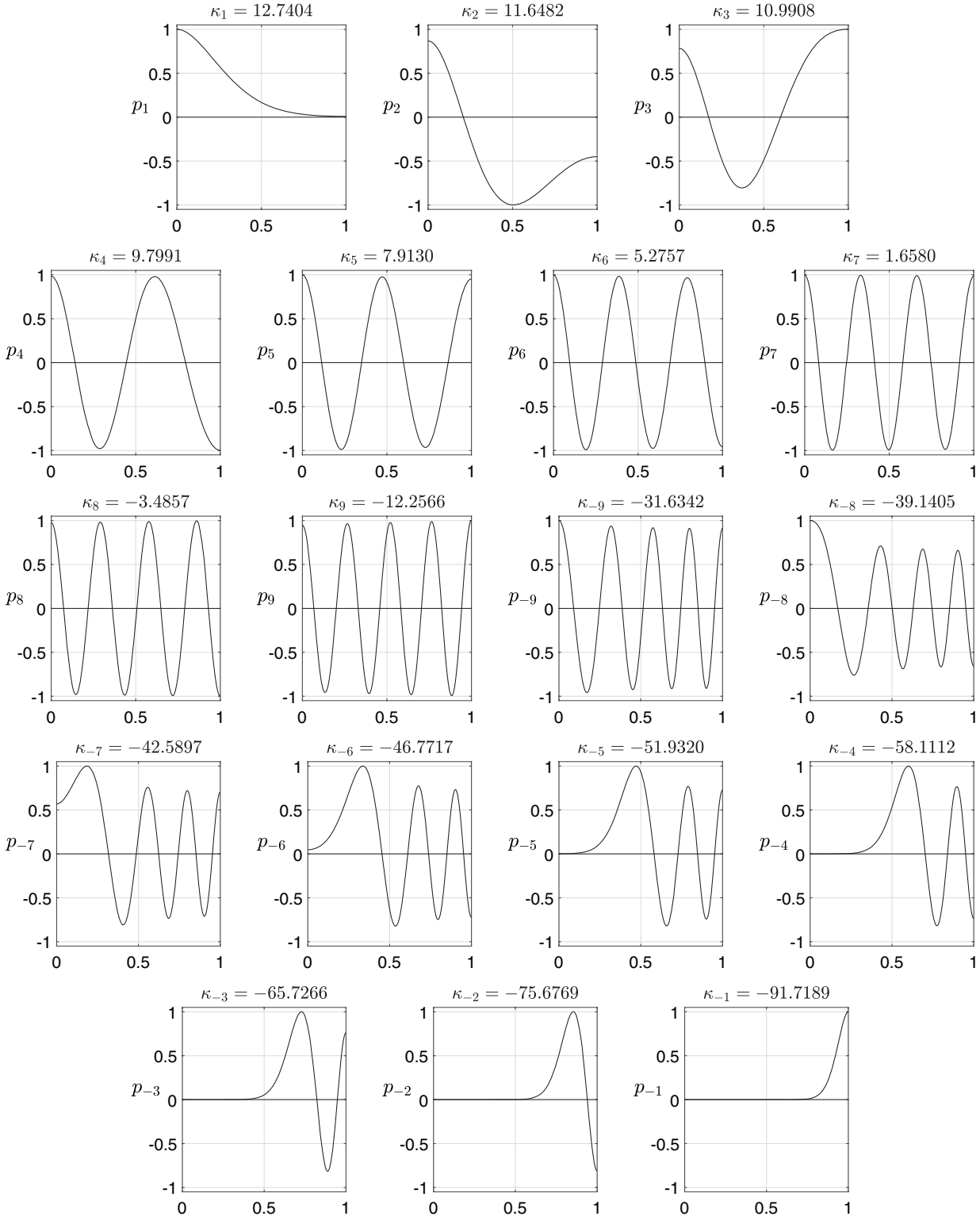

Fig. 3 Eighteen eigenfunction profiles for 2D, hard wall, $\omega = 20$, linear mean flow $u_0 = 0.5 + 0.3y$. Right-running (positive index) and left-running (negative index). Compare with Table 2 and Fig. 4.

for large ω, $r = O(1)$ and $m = O(1)$. Large m, in particular $m = O(\omega)$, is also possible but with some adaptations. We postulate cut-on modes for real κ not near resonance, that is, $\kappa = O(\omega)$ and $\Omega = O(\omega)$. We make the WKB–Ansatz (with phase function $\gamma = O(\omega)$ to be determined)

$$p(r) = A(r)\mathrm{e}^{-\mathrm{i}\int\gamma(z)\,\mathrm{d}z} \tag{76}$$

such that

$$(-\gamma^2+\Omega^2-\kappa^2)A-\frac{\mathrm{i}\Omega^2}{rA}\left(\frac{r\gamma A^2}{\Omega^2}\right)'+\frac{\Omega^2}{r}\left(\frac{rA'}{\Omega^2}\right)'-\frac{m^2}{r^2}A=0 \tag{77}$$

To order $O(\omega^2)$, this leads to

$$\gamma = \sqrt{\Omega^2-\kappa^2} \tag{78}$$

(with a suitably chosen sign) and to order $O(\omega)$

$$A = Q\frac{\Omega}{\sqrt{r\gamma}} \tag{79}$$

with Q a constant. Altogether we have the approximation

$$p(r) \simeq \frac{\Omega}{\sqrt{r\gamma}}\left(Q\mathrm{e}^{-\mathrm{i}\int_0^r\gamma(z)\,\mathrm{d}z}+R\mathrm{e}^{\mathrm{i}\int_0^r\gamma(z)\,\mathrm{d}z}\right) \tag{80}$$

with Q, R, and κ to be determined.

We start with the situation that $\gamma^2 = \Omega^2 - \kappa^2$ is positive along the interval $[0, 1]$, or has a single zero at radial turning point $r_2(\kappa) < 1$, which is such that γ^2 is positive along $[0, r_2]$ and negative along the remaining $[r_2, 1]$.

Near the origin the solution breaks down, and we have to consider a local analysis. Scale

$$r = \omega^{-1}z, \qquad \gamma(0) = \omega\alpha, \qquad z = O(1), \qquad p(r) = P(z) \tag{81}$$

and substitute in the equation, then we get to leading order

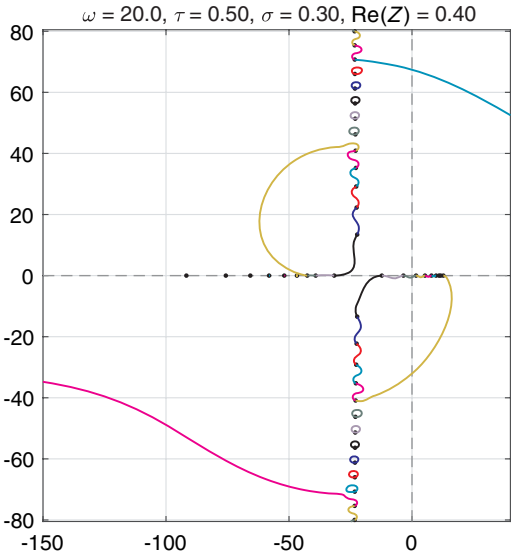

a) Impedance at $y = 0$

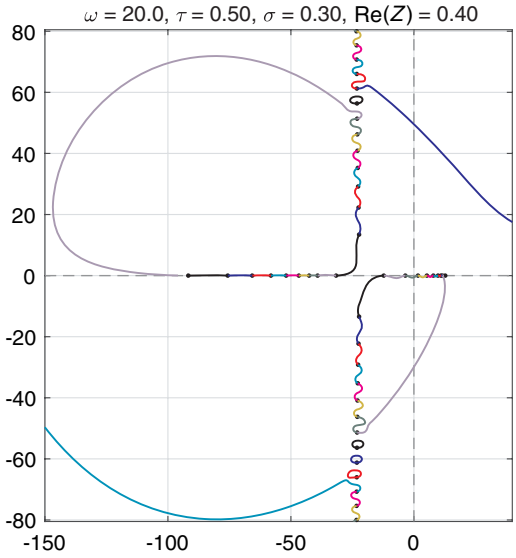

b) Impedance at $y = 1$

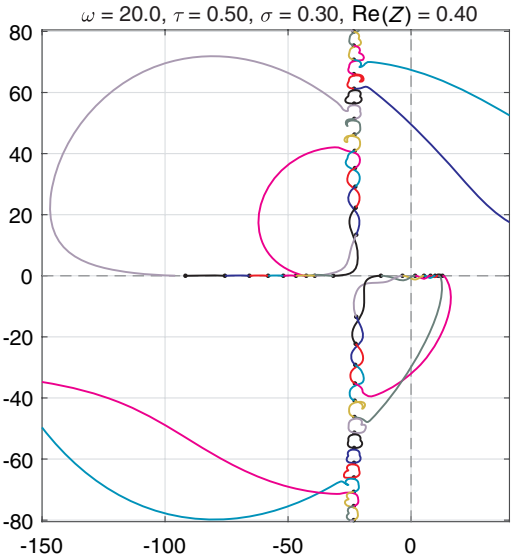

c) The same impedance at both ends

Fig. 4 Two-dimensional, complex wave numbers κ_n for $\omega = 20$, linear profile $u_0 = 0.5 + 0.3y$, $N = 60$, $J = 160$. One or both sides with impedance Z. Tracing for fixed $\mathrm{Re}(Z) = 0.4$ and varying $\mathrm{Im}(Z)$. Compare with Table 2 and Fig. 3.

$$\omega^2 P_{zz} + \omega^2 \frac{1}{z} P_z + \omega^2 \left(\alpha^2 - \frac{m^2}{z^2} \right) P + \cdots = 0 \tag{82}$$

This has the regular solution (a multiple of)

$$P(z) = J_m(\alpha z) \tag{83}$$

which has to match with the WKB approximation. By taking $u_0'(r) \leqslant O(r)$, z large and r small, we find

$$J_m(\alpha z) \simeq \frac{1}{\sqrt{\frac{1}{2}\pi\alpha z}} \cos\left(\alpha z - \frac{1}{4}\pi - \frac{1}{2} m\pi \right)$$
$$\sim \frac{\Omega(0)}{\sqrt{r\omega\alpha}} (Q \mathrm{e}^{-\mathrm{i}\omega\alpha r} + R \mathrm{e}^{\mathrm{i}\omega\alpha r}) \tag{84}$$

So with

$$Q \sim \mathrm{e}^{\frac{1}{4}\pi\mathrm{i} + \frac{1}{2} m\pi\mathrm{i}}, \qquad R \sim \mathrm{e}^{-\frac{1}{4}\pi\mathrm{i} - \frac{1}{2} m\pi\mathrm{i}} \tag{85}$$

the WKB approximation for $r > O(\omega^{-1})$ becomes

$$p(r) \simeq \frac{\Omega(r)}{\sqrt{r\gamma}} \cos\left(\int_0^r \gamma(z)\, \mathrm{d}z - \frac{1}{4}\pi - \frac{1}{2} m\pi \right) \tag{86}$$

An eigenvalue κ for a hard-wall mode is then (to leading order) given by $p'(1) = 0$ or

$$\int_0^1 \gamma(z)\, \mathrm{d}z = \left(n + \frac{1}{4} + \frac{1}{2} m \right) \pi \tag{87}$$

for integer n and provided that there is no radial turning point r_2 along $[0, 1]$. With a turning point r_2 we have to take into account the fact that the solution is exponentially small along $(r_2, 1]$ where γ is imaginary. As a result, only the first interval is considered, Furthermore, matching with the exponentially decaying solution in $[r_2, 1]$ yields a slight change of the effective interval to the effect that we have an extra $\frac{1}{4}\pi$ in the condition

$$\int_0^{r_2} \gamma(z)\, \mathrm{d}z = \left(n + \frac{1}{2} + \frac{1}{2} m \right) \pi \tag{88}$$

for integer n and $r_2 = r_2(\kappa)$. Like before in the 2D case, this condition is (asymptotically) independent of the behavior near $r = 1$. So for any other boundary condition at the wall the solution, including the value of κ, is the same. In other words, the effect of the wall is shielded by turning point r_2.

If γ^2 has a zero $r_1(\kappa)$ along $[0, 1]$ such that γ^2 is negative along $[0, r_1]$ and positive along $[r_1, 1]$, the singularity at $r = 0$ plays no role because the solution is exponentially small anyway. We have to consider the second interval $[r_1, 1]$, including the same slight change of the effective interval due to matching with the exponentially decaying solution in $[0, r_1]$ as before. We obtain the approximation

$$p(r) \simeq \frac{\Omega}{\sqrt{r\gamma}} \sin\left(\int_{r_1}^r \gamma(z)\, \mathrm{d}z + \frac{1}{4}\pi \right) \tag{89}$$

which leads, due to the boundary condition $p'(1) = 0$, to the eigenvalue condition

$$\int_{r_1}^1 \gamma(z)\, \mathrm{d}z = \left(n + \frac{1}{4} \right) \pi \tag{90}$$

for integer n and $r_1 = r_1(\kappa)$. For other configurations similar arguments apply. Note that the approximation deteriorates if ω is not large, m is too large, and r_1 or r_2 are too close to 0, 1 or each other. All these bordering situations can be treated on a case-by-case basis, but on the whole that is not necessary to understand the major trends and global behavior that appear from the numerical solution.

VI. Examples and Applications

The first results are centered around the 2D problem with the linear mean flow profile $u_0 = \tau + \sigma y$, $\tau = 0.5$, $\sigma = 0.3$; a relatively high frequency, $\omega = 20$; and no sound speed variation, $c_0 = 1$. In Table 2 a comparison is made of the 2×9 cut-on modal wave numbers, found numerically (with $N = 40$ Chebyshev basis functions and $J = 80$ Gauss–Legendre nodes) and by WKB. The agreement is very satisfactory, although depends on secondary effects like the distance between the walls and the turning points

$$y_1 = \frac{\omega + \kappa - \kappa\tau}{\kappa\sigma}, \qquad y_2 = \frac{\omega - \kappa - \kappa\tau}{\kappa\sigma}$$

Observe that the first two right-running modes have turning points y_2 and decay near $y = 1$, and the first seven left-running modes have turning points at y_1 and decay near $y = 0$. This is confirmed by Fig. 3, where the modal shapes are given. The first right-running mode practically vanishes at $y = 1$, and the first five or six left-running modes practically vanish at $y = 0$. This may cause these modes to be insensitive to an impedance placed at the side where the mode vanishes. This happens, for example, in the two cases given in Figs. 4a and 4b, where one side is hard and the other soft, and vice versa. The modes are traced from their hard-wall values for varying impedances, with fixed real parts (0.4) and imaginary parts varying from ∞ to $-\infty$, while $N = 60$ and $J = 160$. We see that the first right-running mode is (practically) insensitive to the impedance at $y = 1$, and the first 6 left-running modes are insensitive to the impedance at $y = 0$. The insensitive modal wave numbers vary along very small circles. In the plot these appear like points.

Associated to the respective impedance, four surface waves develop with mean flow profiles with slip [8] (six with a thin boundary layer [10]). Here we have two impedances and slip. So we expect eight surface modes. Because they live in different

Table 3 Comparison of 16 cut-on hard-wall modes

	Numerical	WKB		
n	κ_n	κ_n	r_1	r_2
	a) $[r_1, 1]$			
1	+13.9204	+13.8400	0.8425	
2	+11.6581	+11.6915	0.4227	
	b) $[0, 1]$			
3	+10.3427	+10.2436		
4	+8.6215	+8.5506		
5	+6.1758	+6.1112		
6	+2.7973	+2.7321		
7	−1.9877	−2.0617		
8	−9.8657	−9.9806		
	c) $[0, r_2]$			
−1	−89.9857	−90.0412		0.2103
−2	−80.1206	−80.1827		0.3144
−3	−70.3901	−70.4604		0.4095
−4	−60.8468	−60.9274		0.5065
−5	−51.5706	−51.6641		0.6117
−6	−42.6829	−42.7924		0.7313
−7	−34.4697	−34.4942		0.8716
−8	−28.4241	−27.0191		1.0394

WKB approximation and numerical solution ($N = 40$ even Chebyshev polynomials, $J = 80$); 3D circular duct; $\omega = 20$, $m = 1$; parabolic mean flow profile $u_0 = 0.8 - 0.5r^2$ and $c_0 = 1$; turning points at r_1 and r_2.

mean flow velocities, they develop differently. In the combined case of Fig. 4c, where both ends have the same impedance, indeed eight surface waves develop, practically following the same tracks as in Eqs. (4a) and (4b), confirming that they are associated to one wall, independent of the opposite side. The regular acoustic modes, on the other hand, live in the whole duct and differ in the three cases.

A study, similar to the one above but now in 3D, is given in Table 3 and Fig. 5, with $N = 40$, $J = 80$. A parabolic mean flow profile $u_0 = \tau - \sigma r^2$, $\tau = 0.8$, $\sigma = 0.5$, and constant sound speed $c_0 = 1$ is considered for modes of frequency $\omega = 20$, $m = 1$, and associated turning points

$$r_1 = \left(\frac{\kappa\tau + \kappa - \omega}{\kappa\sigma}\right)^{\frac{1}{2}}, \qquad r_2 = \left(\frac{\kappa\tau - \kappa - \omega}{\kappa\sigma}\right)^{\frac{1}{2}}$$

The agreement between numerical and WKB modal wave numbers (Table 3) is very satisfactory, except for κ_{-8} because of turning point r_2 being close to one. The effect of the local approximation near $r = 0$ is well captured. The first two right-running modes have turning points at r_1 and decay toward $r = 0$, and the first seven or eight left-running modes have turning points at r_2 and decay toward the wall $r = 1$. This is confirmed by the modal shape plots in Fig. 5. The first six or seven (left-running) upstream running modes practically vanish at $r = 1$, with the result that these modes are almost insensitive to the wall impedance. This is well illustrated in the modal trace plots of Fig. 6 for $\mathrm{Re}(Z) = 0.1$.

Although modes remain self-similar in the axial direction and by themselves do not refract, this insensitivity may be interpreted as a manifestation in the modal spectrum of rays refracting into regions with a lower effective sound speed, and away from regions with a higher effective sound speed [1], [40] (Sec. 16.9). With a mean flow,

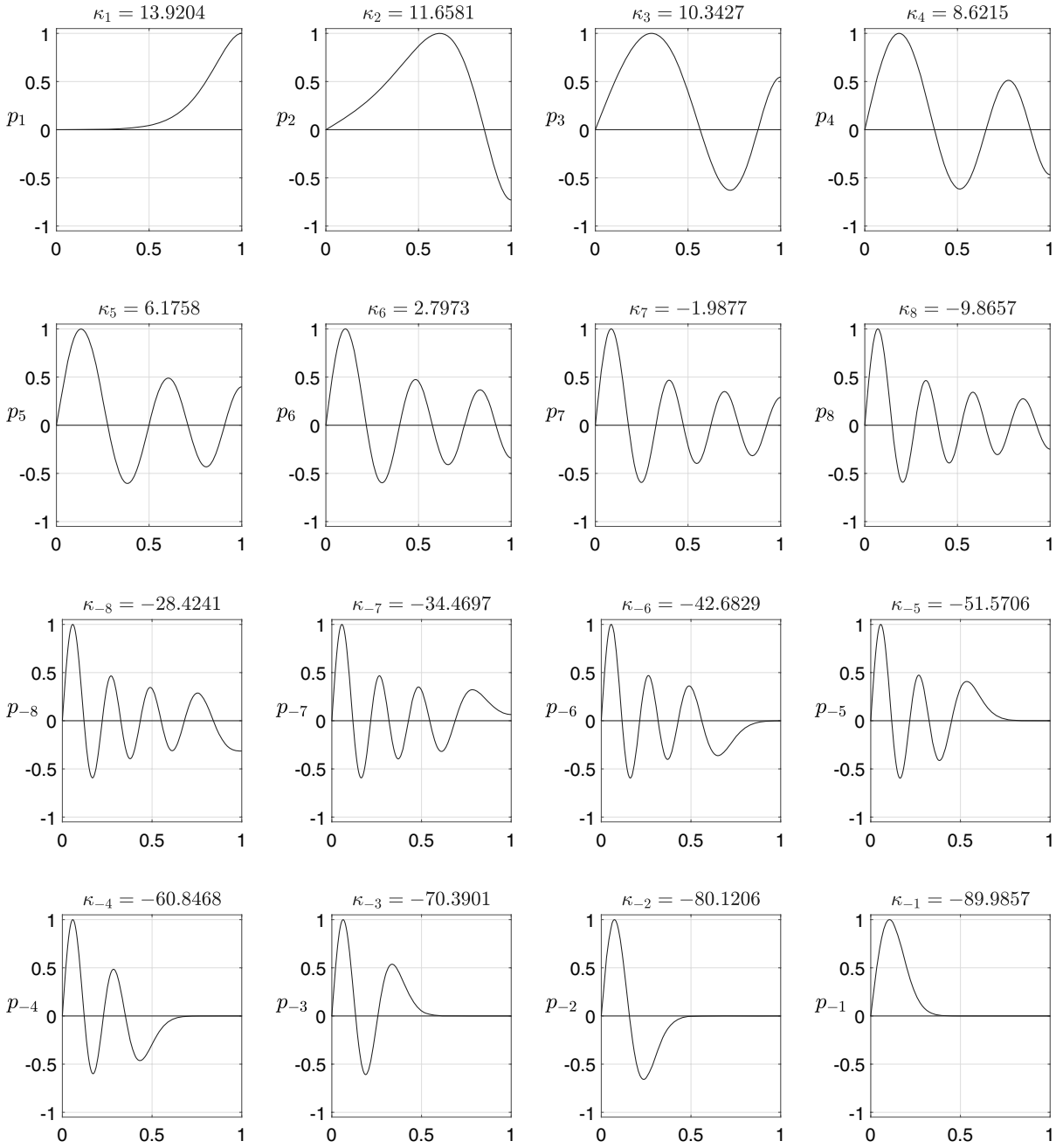

Fig. 5 Eigenfunction profiles for 3D, hard wall, $\omega = 20$, $m = 1$, parabolic $u_0 = 0.8 - 0.5r^2$. Right-running (positive index) and left-running (negative index). Compare with Table 3.

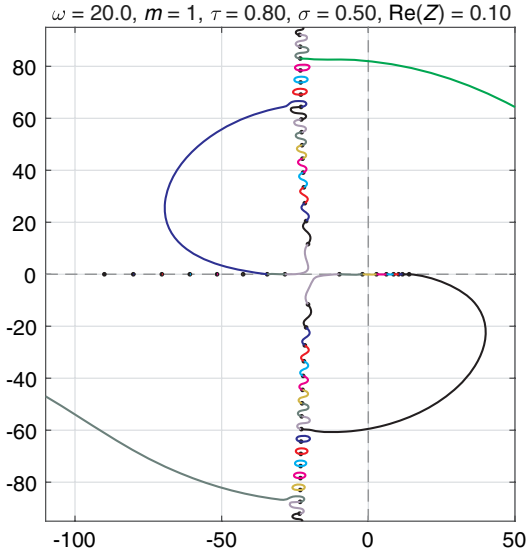

Fig. 6 Three-dimensional, complex wave numbers κ_{mn} for $\omega = 20$, $m = 1$, and parabolic profile $u_0 = 0.8 - 0.5r^2$. Tracing for varying $\mathrm{Im}(Z)$ and fixed $\mathrm{Re}(Z) = 0.1$. Compare with Table 3 and Fig. 5.

vanishing at the wall, the effective sound speed $c_0 \pm u_0$ depends on the direction of the sound, and so downstream modes will refract to the wall and upstream modes away from the wall.

In Fig. 7, 3D modes of $\omega = 5$, $m = 0$, $c_0 = 1$ and parabolic profiles $u_0 = \tau - \sigma r^2$, $\tau = 0.75$, and $\sigma = 0.75$ (no slip flow; left) and $\sigma = 0.25$ (slip flow; right) are traced with $\mathrm{Im}(Z)$ and fixed $\mathrm{Re}(Z) = 0.01$. The relatively small value of $\mathrm{Re}(Z)$ is not a problem numerically, even with the moderate number of basis functions ($N = 40$) and Gauss–Legendre nodes ($J = 80$) that has been used. The well-known structure of regular modes, and acoustic and hydrodynamic surface waves for uniform mean flow [8,9] is also present for parabolic profiles with slip flow, but without slip the hydrodynamic surface waves are not present, as there is indeed no mean flow at the wall. However, the presence of the mean flow in the rest of the duct requires a left-running first modal wave number of $\kappa_{-1} \simeq -14.795$, which makes the square root $\sqrt{\Omega^2 - \kappa^2}$ imaginary near $r = 1$ and therefore the mode shape exponentially small. Indeed this mode is insensitive to the impedance, and the corresponding acoustic surface wave develops from κ_{-2}, rather than κ_{-1}.

Because the boundary condition for vanishing boundary layer (3) (the so-called Ingard limit [15]) is known to be sensitive, at least for the (altogether six) surface waves [10,18], it is of interest to check the behavior of the numerical solution for the decreasing boundary-layer thickness. A series of cases is presented in Fig. 8, where 3D modes of $\omega = 5$, $m = 0$ are traced (with $N = 40$, $J = 80$) along $\mathrm{Re}(Z) = 0.1$ in an almost uniform mean flow of $u_0 \simeq 0.5$ given by Eq. (C2), and boundary layers of typical thickness $\delta = 0.1$, 0.05, 0.01, and 0. The regular acoustic modes and the right-running acoustic surface wave in the fourth quadrant are easily reproduced. The other surface waves converge poorly. With $\delta = 0.1$–0.01 a left-running surface wave is seen in the second quadrant that does not converge to the acoustic surface wave for $\delta = 0$, and is a surface wave of the type predicted by Brambley [10], resulting from interaction with the thin boundary layer. Another "boundary-layer interaction" surface wave is seen in the first quadrant for $\delta = 0.05$. This one turns via $\delta = 0.01$ into a hydrodynamic surface wave for $\delta = 0$. The other hydrodynamic surface wave in the third quadrant is only seen for $\delta = 0$.

For the surface waves in the first and third quadrant we cannot expect an easy convergence, because the real parts of κ tend to infinity, and this implies a nonuniform limit with $\delta \to 0$. For example, near $y = 0$ a first quadrant surface wave behaves like

$$p \sim \mathrm{e}^{\pm \mathrm{i}\sqrt{\Omega^2 - \kappa^2}\,y} \simeq \mathrm{e}^{-\sqrt{1-u_0^2}\kappa y}$$

The Ingard limit assumes a boundary-layer thickness much less than the typical width of the mode, which means that $\delta\kappa \ll 1$, and so the limit is not valid for $\kappa \gtrsim \delta^{-1}$. Indeed, for $\delta = 0.01$ the calculation of the first quadrant surface wave became unstable for $\kappa > 20$ and needed a large number of Gauss–Legendre points to stabilize (we used $N = 60$, $J = 4000$). No surface mode for any $\delta > 0$ was found in the third quadrant. Maybe a much smaller value of δ is necessary, but this appeared difficult to realize.

Another investigation of the effect of a boundary layer is presented in Fig. 9, where the two cut-on hard wall modes of rotor-alone noise of a 22-blade rotor with periodicity $m = 22$ and blade passing frequency ω varying around $\omega = 22$ is studied in an almost uniform mean flow [$u_0 \simeq 0.6$, Eq. (C2)] as a function of boundary layer $\delta = 0 \ldots 0.1$ in steps of 0.01 ($N = 40$, $J = 200$). It is seen that at $\omega = 22$ and $\delta = 0$ the modes are well cut-on, but when δ is increased,

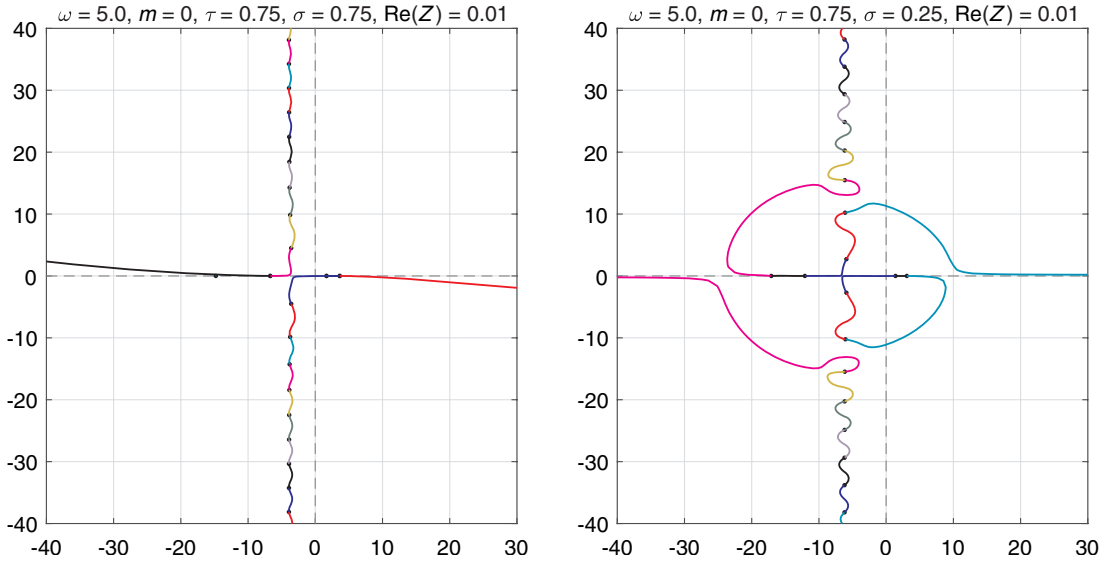

Fig. 7 Three-dimensional, complex wave numbers κ_n for $\omega = 5$, $m = 0$, and parabolic profiles with no slip $u_0 = 0.75 - 0.75r^2$ (left) and slip $u_0 = 0.75 - 0.25r^2$ (right). Tracing for varying $\mathrm{Im}(Z)$ and fixed small $\mathrm{Re}(Z) = 0.01$.

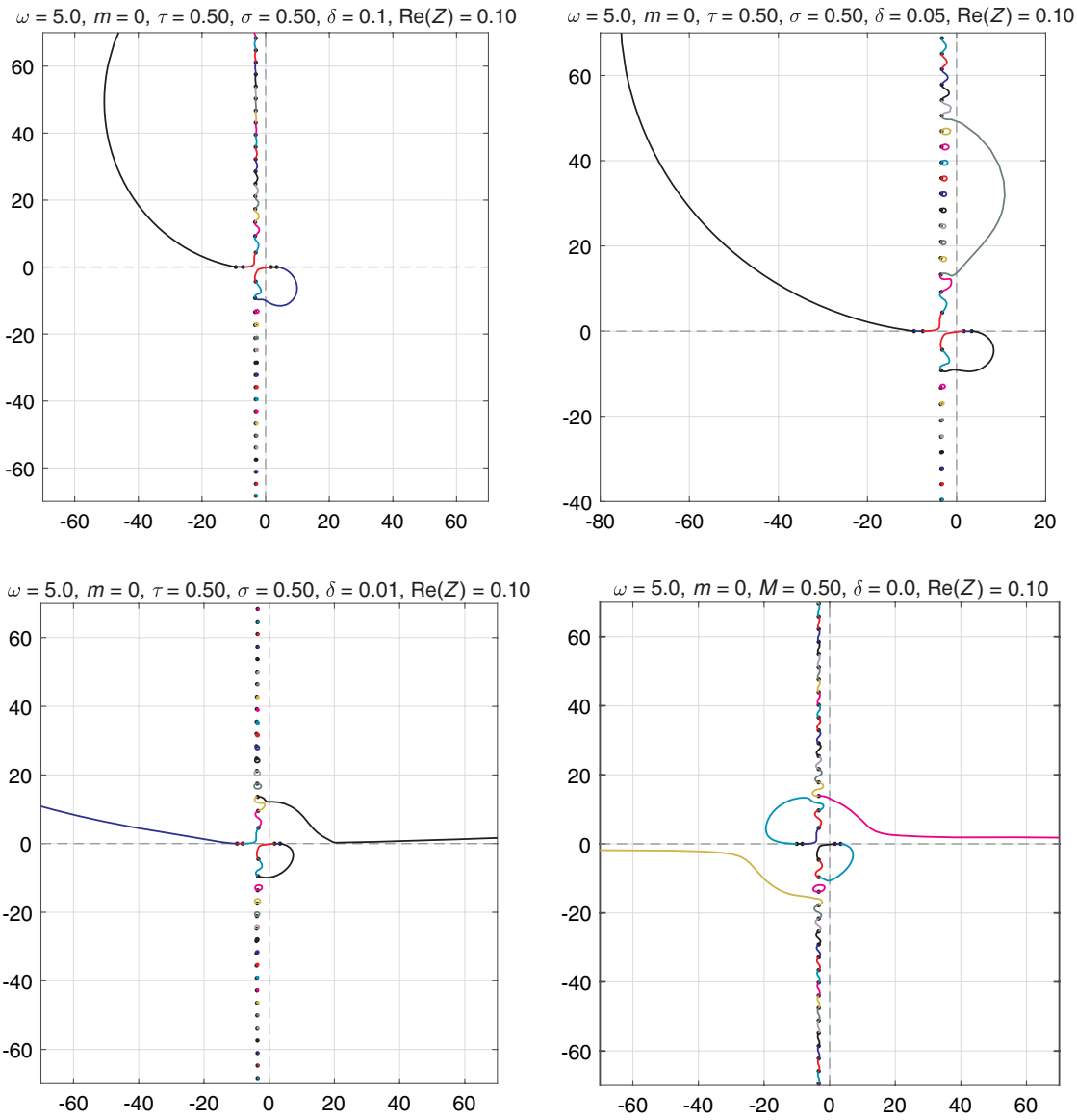

Fig. 8 Three-dimensional, complex wave numbers κ_n for $\omega = 5$, $m = 0$ and almost uniform profile [Eq. (C2)] with $\tau = \sigma = 0.5$ and boundary layers of $\delta = 0.1$, $= 0.05$, $= 0.01$, $= 0.0$ ($\delta = 0$ uses the Ingard limit). Tracing for varying $\mathrm{Im}(Z)$ and fixed $\mathrm{Re}(Z) = 0.1$.

the modes become cutoff for $\delta > 0.055$. So the presence of rotor-alone noise greatly depends on details of the boundary layer (and the mean flow Mach number, of course).

In Fig. 10, 3D cut-on hard-wall modes are plotted as a function of frequency, with centerline Mach number ∼0.9. We see that with a parabolic profile (right) there is a qualitative difference between low and high frequencies, which is not present with a uniform profile (left). This is caused by the fact that with the parabolic profile and high ω the first few (left- and right-running) modes are nonuniformly distributed in the duct (see, e.g., Fig. 5), making them more susceptible to mean flow variations. This is not possible with low ω. The low ω approximation of Eq. (49a) is given as a dotted line. For the uniform profile, this happens to be exact for the first (κ_1 and κ_{-1}) mode. For the parabolic profile, the agreement is very reasonable for $\omega < 2$.

Finally, in Fig. 11 some (relatively) low-frequency 3D modes with impedance walls and parabolic mean flow profiles are traced in Z for various fixed $\mathrm{Re}(Z)$, whereas the low ω approximation, given by Eq. (52), is included as dotted lines. Consistent with the assumed scaling $Z = O(\omega^{-1})$, the approximation is especially very good near the hard wall limits. Otherwise, as long as the mode does not become a surface wave, the agreement is very reasonable.

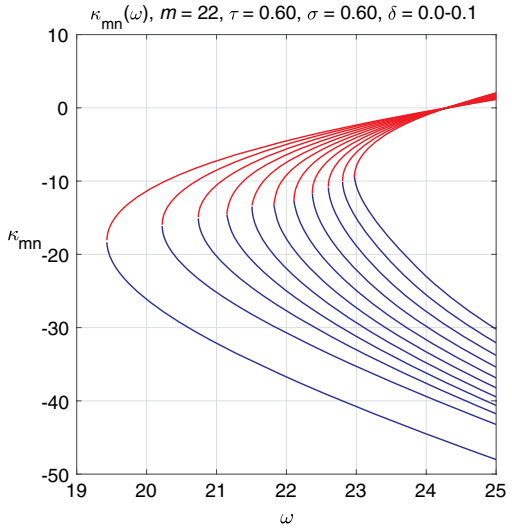

Fig. 9 Three-dimensional, cut-on wave numbers κ_{m1} (red) and $\kappa_{m,-1}$ (blue) versus frequency ω and boundary layer δ. $19 \leqslant \omega \leqslant 25$, $m = 22$. Almost uniform profile u_0 [Eq. (C2)] with $\tau = \sigma = 0.6$ and boundary layer varying between $\delta = 0.0$ and 0.1 from left to right in steps of 0.01.

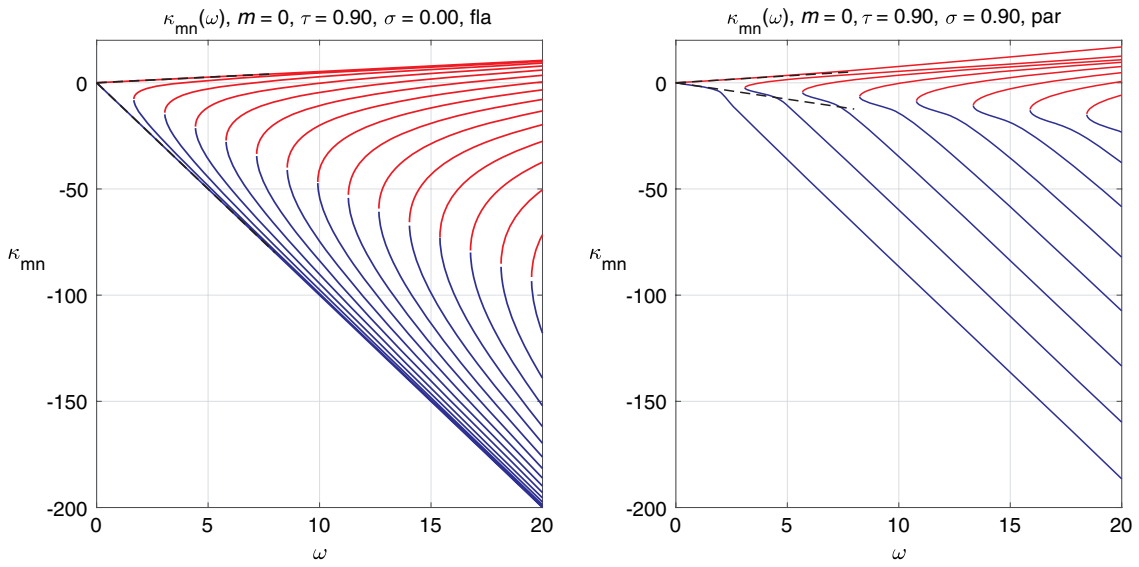

Fig. 10 Three-dimensional, cut-on wave numbers κ_{mn} versus frequency ω. $0 \leqslant \omega \leqslant 20$, $m = 0$. Comparison of uniform profile $u_0 = 0.9$ (left), and parabolic profile $u_0 = 0.9 - 0.9r^2$ (right); ——: right-running; ——: left-running. Dashed lines: $\omega \ll 1$ approximation [Eq. (49a)].

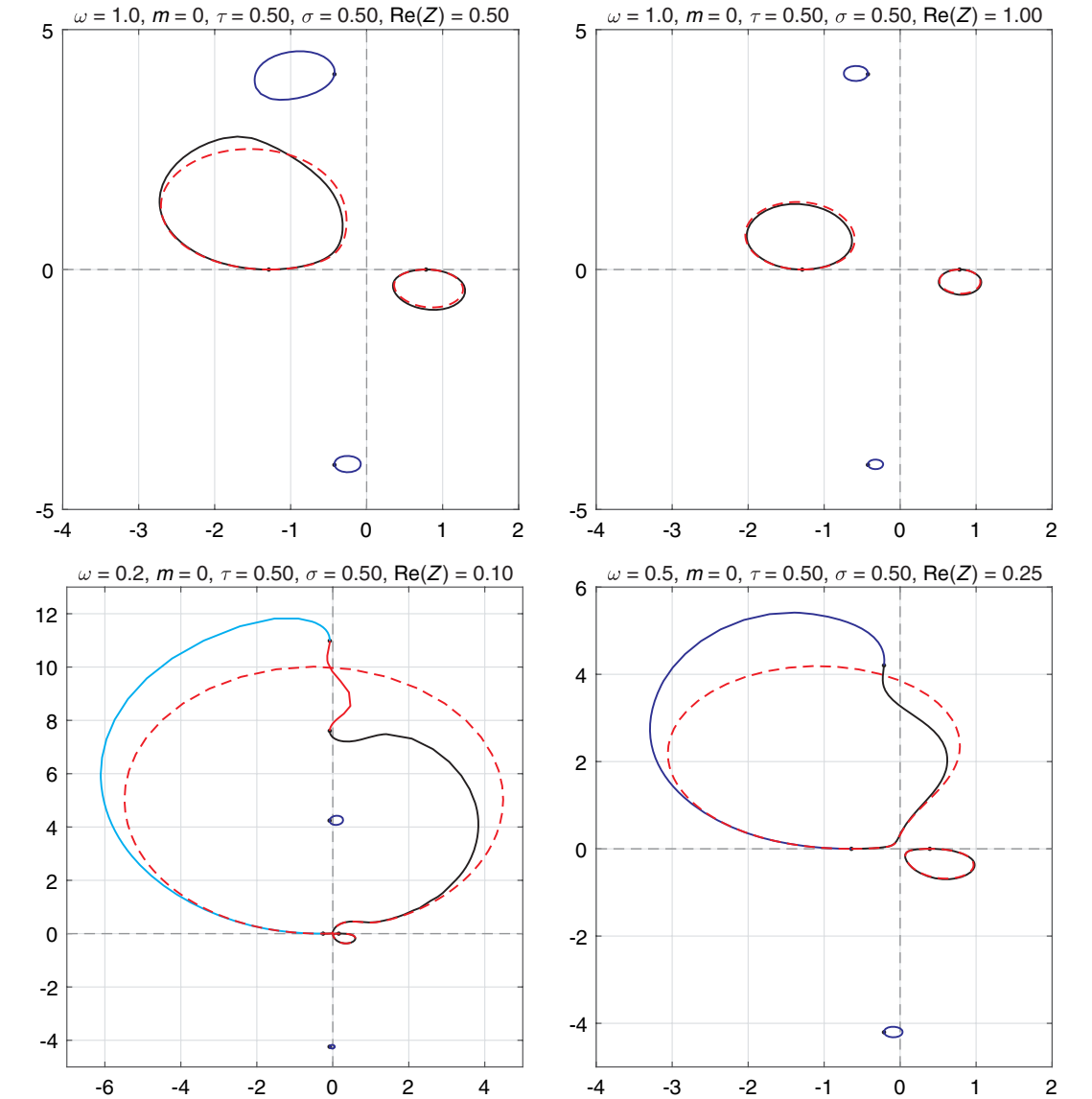

Fig. 11 Three-dimensional, complex wave numbers κ_n of small ω, $m = 0$, and parabolic $u_0 = 0.5 - 0.5r^2$. Tracing for varying $\mathrm{Im}(Z)$ and fixed $\mathrm{Re}(Z)$. $N = 20$, $J = 40$. Dashed lines: $\omega \ll 1$ approximation [Eq. (52)].

VII. Conclusions

Duct acoustics is an important part of aeroacoustics, as it relates to the generation, propagation, radiation, and attenuation of turbine and rotor–stator interaction noise of aeroengines. Many features are described, or at least understood and clarified, by the concept of modes, a wave form that emerges naturally if the duct can be modeled as straight with a plane parallel mean flow and constant wall properties.

In the present paper we have studied duct modes for nonuniform mean flow profiles, described by Pridmore-Brown equations. The 2D Pridmore-Brown equation has been studied in a duct with lined walls both at the top and at the bottom, and the 3D Pridmore-Brown equation in a hollow cylindrical duct with a lined wall.

Numerical solutions have been constructed based on a Galerkin projection with a Chebyshev function basis (except for the situation with $Z = 0$), leading to a nonlinear eigenvalue problem that has been solved by an effective Newton-type routine. Analytical asymptotic approximations have been constructed for low and high frequencies ω.

Except for $Z = 0$, the wave number of the first modes is $O(\omega)$ for small ω, and after scaling a formal asymptotic solution could be given. For simple enough mean flow profiles this solution can be evaluated entirely analytically, with very favorable agreement with the numerical solution. The found expressions for the wave numbers in 2D with a linear profile and in 3D with a parabolic profile show interesting similarities.

For high frequencies the WKB method can be invoked successfully. A most interesting feature, displayed by the WKB solution, is the possibility of a transverse turning point that separates the acoustic part of the solution from an exponentially small part near the wall. In this way the solution may in some cases be insensitive to the impedance condition. This happens with parabolic flow profiles for upstream running modes, and for both left- and right-running modes in a medium with concave-type sound speed profiles. This is by and large in agreement with the ray-acoustic rule that sound refracts in the direction of the lowest effective sound speed. If this occurs, eduction of the wall impedance from acoustic measurements will be impossible, at least if the insensitive modes dominate the sound field.

Surface waves are present both with uniform and nonuniform flow. They are well-captured numerically, including the type, predicted by Brambley [10], caused by interaction with a thin boundary layer. Only the combined limit of boundary layer $\delta \to 0$ and $Z \to \infty$, such that surface wave number $\kappa \to \infty$, is nonuniform and more difficult numerically. Perhaps for this particular problem another numerical method is preferable.

Appendix A: Preparatory Manipulations to the Pridmore-Brown Equations

The isentropic Euler equations for a perfect gas, with velocity $\boldsymbol{v}$, pressure p, density ρ, sound speed c, entropy s, constant heat capacities C_P, C_V and their ratio γ, small mass source q', and small force $\boldsymbol{f}'$, are

$$\frac{\mathrm{d}\rho}{\mathrm{d}t} + \rho\nabla\cdot\boldsymbol{v} = q', \qquad \rho\frac{\mathrm{d}\boldsymbol{v}}{\mathrm{d}t} + \nabla p = \boldsymbol{f}',$$
$$\frac{\mathrm{d}s}{\mathrm{d}t} = \frac{C_V}{p}\left(\frac{\mathrm{d}p}{\mathrm{d}t} - c^2\frac{\mathrm{d}\rho}{\mathrm{d}t}\right) = 0, \qquad c^2 = \gamma\frac{p}{\rho} \tag{A1}$$

Consider a mean flow $\boldsymbol{v}_0, p_0, \rho_0, c_0$ with perturbations $\boldsymbol{v}', p', \rho'$ due to q' and $\boldsymbol{f}'$. If the mean flow is plane parallel with $p_0 = \rho_0 c_0^2/\gamma$ a constant, $\boldsymbol{v}_0 = u_0\boldsymbol{e}_x$, while u_0, ρ_0, c_0 only depend[‡‡] on y, z, then the mean flow satisfies the stationary Euler equations. For the perturbations we have after linearization

$$D_0\rho' + \boldsymbol{v}'\cdot\nabla\rho_0 + \rho_0(\nabla\cdot\boldsymbol{v}') = q' \tag{A2a}$$

$$\rho_0 D_0\boldsymbol{v}' + \rho_0(\boldsymbol{v}'\cdot\nabla u_0)\boldsymbol{e}_x + \nabla p' = \boldsymbol{f}' \tag{A2b}$$

$$D_0 p' - c_0^2 D_0\rho' - c_0^2(\boldsymbol{v}'\cdot\nabla\rho_0) = 0 \tag{A2c}$$

where the convective derivative is $D_0 = (\partial/\partial t) + u_0(\partial/\partial x)$. Following [2], [42] (page 10), we take the convective derivative of the divergence of Eq. (A2b), which becomes, with (A2a) and the y, z components of (A2b)

$$-c_0^2 D_0^3\rho' - 2c_0^2\frac{\partial}{\partial x}(\nabla p'\cdot\nabla u_0) + D_0(c_0^2\nabla^2 p')$$
$$= c_0^2 D_0\nabla\cdot\boldsymbol{f}' - c_0^2 D_0^2 q' - 2c_0^2\frac{\partial}{\partial x}(\boldsymbol{f}'\cdot\nabla u_0)$$

Further elaboration [use the fact that $\rho_0 c_0^2$ is a constant, and then Eq. (A2c)] yields the wave equation

$$D_0\nabla\cdot(c_0^2\nabla p') - D_0^3 p' - 2c_0^2\frac{\partial}{\partial x}(\nabla p'\cdot\nabla u_0)$$
$$= -c_0^2 D_0^2 q' + D_0\nabla\cdot(c_0^2\boldsymbol{f}') - 2c_0^2\frac{\partial}{\partial x}(\boldsymbol{f}'\cdot\nabla u_0) \tag{A3}$$

Without the forcing terms we can assume modes of the form $p'(\boldsymbol{x}, t) = \hat{p}(y, z)\mathrm{e}^{\mathrm{i}\omega t - \mathrm{i}\kappa x}$. With the forcing terms we apply Fourier transformation

$$p'(x, y, z, t) = \frac{1}{2\pi}\int_{-\infty}^{\infty}\hat{p}(y, z)\mathrm{e}^{\mathrm{i}\omega t - \mathrm{i}\kappa x}\,\mathrm{d}\kappa$$

such that $(\partial/\partial x) \to -\mathrm{i}\kappa$ and $D_0 \to \mathrm{i}(\omega - \kappa u_0) = \mathrm{i}c_0\Omega$, while for clarity we denote by $\tilde{\nabla}$ the nabla operator restricted to y and z. We get eventually the preform of the Pridmore-Brown equations:

$$\Omega^2\tilde{\nabla}\cdot\left(\frac{1}{\Omega^2}\tilde{\nabla}\hat{p}\right) + (\Omega^2 - \kappa^2)\hat{p} = -\mathrm{i}c_0\Omega q' - \mathrm{i}\kappa\hat{\boldsymbol{f}}\cdot\boldsymbol{e}_x + \Omega^2\tilde{\nabla}\cdot\left(\frac{1}{\Omega^2}\hat{\boldsymbol{f}}\right) \tag{A4}$$

Appendix B: Exact Integrals

Among other things, exact results for the Pridmore-Brown modes are very useful to check and verify the numerical routines. Therefore we give here a few.

By integrating the differences $g(\text{equation for} f) - f(\text{equation for} g)$ of two independent solutions f and g of Eq. (6), respectively, Eq. (8), we find in 2D and 3D the Wronskians

$$fg' - gf' = C\Omega^2, \qquad fg' - gf' = C\frac{\Omega^2}{r} \tag{B1}$$

where C are constants depending on f and g.

In a similar way, for two different solutions p_1 and p_2 with all parameters the same, except the eigenvalues κ_1 and κ_2 and impedances Z_{01} and Z_{02} at $y = 0$, and Z_{11} and Z_{12} at $y = 1$, we can derive in 2D

$$\int_0^1\left(\frac{F}{\Omega_1^2} - \frac{G}{\Omega_2^2}\right)p_1' p_2' + \left(\frac{F'}{\Omega_1^2}p_1' p_2 - \frac{G'}{\Omega_2^2}p_1 p_2'\right)$$
$$+ \left(F\frac{\kappa_1^2}{\Omega_1^2} - G\frac{\kappa_2^2}{\Omega_2^2} - F + G\right)p_1 p_2\,\mathrm{d}y$$
$$= \frac{1}{\mathrm{i}\omega}\left[\left(\frac{F}{Z_{11}} - \frac{G}{Z_{12}}\right)p_1 p_2\right]_{y=1} + \frac{1}{\mathrm{i}\omega}\left[\left(\frac{F}{Z_{01}} - \frac{G}{Z_{02}}\right)p_1 p_2\right]_{y=0}$$

and in 3D with impedances Z_1 and Z_2 at $r = 1$

[‡‡] If the flow is homentropic, p_0, ρ_0, and c_0 should be constant everywhere.

$$\int_0^1 \left(\frac{F}{\Omega_1^2}-\frac{G}{\Omega_2^2}\right) r p_1' p_2' + \left(\frac{F' r}{\Omega_1^2} p_1' p_2 - \frac{G' r}{\Omega_2^2} p_1 p_2'\right) + \left(\frac{\kappa_1^2}{\Omega_1^2}+\frac{m^2}{r^2\Omega_1^2}-1\right) F p_1 p_2 - \left(\frac{\kappa_2^2}{\Omega_2^2}+\frac{m^2}{r^2\Omega_2^2}-1\right) G p_1 p_2 \,\mathrm{d}r = \left[\left(\frac{F}{\mathrm{i}\omega Z_1}-\frac{G}{\mathrm{i}\omega Z_2}\right) p_1 p_2\right]_{r=1}$$

By choosing F and G we can generate exact integrals. For example, $F = G = 1$ yields

$$\int_0^1 \left(\frac{\kappa_1^2}{\Omega_1^2}-\frac{\kappa_2^2}{\Omega_2^2}\right) p_1 p_2 + \left(\frac{1}{\Omega_1^2}-\frac{1}{\Omega_2^2}\right) p_1' p_2' \,\mathrm{d}y = \frac{1}{\mathrm{i}\omega}\left[\left(\frac{1}{Z_{11}}-\frac{1}{Z_{12}}\right) p_1 p_2\right]_{y=1} + \frac{1}{\mathrm{i}\omega}\left[\left(\frac{1}{Z_{01}}-\frac{1}{Z_{02}}\right) p_1 p_2\right]_{y=0} \tag{B2}$$

and

$$\int_0^1 \left(\frac{\kappa_1^2}{\Omega_1^2}+\frac{m^2}{r^2\Omega_1^2}-\frac{\kappa_2^2}{\Omega_2^2}-\frac{m^2}{r^2\Omega_2^2}\right) p_1 p_2 + \left(\frac{1}{\Omega_1^2}-\frac{1}{\Omega_2^2}\right) r p_1' p_2' \,\mathrm{d}r = \frac{1}{\mathrm{i}\omega}\left[\left(\frac{1}{Z_1}-\frac{1}{Z_2}\right) p_1 p_2\right]_{r=1} \tag{B3}$$

Also interesting is $G = 0$ and $p_1 = p_2$, leading to

$$\int_0^1 F p^2 \,\mathrm{d}y = \int_0^1 \frac{F}{\Omega^2}(\kappa^2 p^2 + p'^2) + \frac{F'}{\Omega^2} p p' \,\mathrm{d}y - \left[\frac{F p^2}{\mathrm{i}\omega Z_1}\right]_{y=1} - \left[\frac{F p^2}{\mathrm{i}\omega Z_0}\right]_{y=0} \tag{B4}$$

and

$$\int_0^1 F p^2 \,\mathrm{d}r = \int_0^1 \frac{F}{\Omega^2}\left(\left(\kappa^2+\frac{m^2}{r^2}\right) p^2 + r p'^2\right) + \frac{F'}{\Omega^2} r p p' \,\mathrm{d}r - \left[\frac{F p^2}{\mathrm{i}\omega Z}\right]_{r=1} \tag{B5}$$

Another integral, essentially the equivalent of the result derived in [24], is in 2D given by

$$\int_0^1 \frac{1}{\Omega_2}\left[\left(\left(1+\frac{\kappa_1\kappa_2}{\Omega_1\Omega_2}\right)\frac{u_0}{c_0}+\frac{\kappa_1}{\Omega_1}+\frac{\kappa_2}{\Omega_2}\right) p_1 p_2 - \frac{\omega u_0'}{c_0^2\Omega_1^2\Omega_2} p_1' p_2 + \frac{u_0}{c_0\Omega_1\Omega_2} p_1' p_2'\right]\mathrm{d}y = \frac{1}{\mathrm{i}\omega(\kappa_1-\kappa_2)}\left[\left[\left(\frac{\Omega_1}{Z_{11}}-\frac{\Omega_2}{Z_{12}}\right)\frac{p_1 p_2}{\Omega_2}\right]_{y=1} + \left[\left(\frac{\Omega_1}{Z_{01}}-\frac{\Omega_2}{Z_{02}}\right)\frac{p_1 p_2}{\Omega_2}\right]_{y=0}\right] \tag{B6}$$

and in 3D by

$$\int_0^1 \frac{r}{\Omega_2}\left[\left(\left(1+\frac{\kappa_1\kappa_2}{\Omega_1\Omega_2}+\frac{m^2}{r^2\Omega_1\Omega_2}\right)\frac{u_0}{c_0}+\frac{\kappa_1}{\Omega_1}+\frac{\kappa_2}{\Omega_2}\right) p_1 p_2 - \frac{\omega u_0'}{c_0^2\Omega_1^2\Omega_2} p_1' p_2 + \frac{u_0}{c_0\Omega_1\Omega_2} p_1' p_2'\right]\mathrm{d}r = \frac{1}{\mathrm{i}\omega(\kappa_1-\kappa_2)}\left[\left(\frac{\Omega_1}{Z_1}-\frac{\Omega_2}{Z_2}\right)\frac{p_1 p_2}{\Omega_2}\right]_{r=1} \tag{B7}$$

Appendix C: A Family of Flow Profiles with Boundary Layer

To obtain a flow profile in a cylindrical duct such that the boundary layer has exponential decay, the behavior in the origin is smooth, and the displacement and momentum thicknesses are explicitly available, we could try [18]

$$U(r) = \tanh\left(\frac{1-r}{\delta}\right) + a + br + cr^2$$

With the conditions $U(0) = 1$, $U(1) = 0$, and $U'(0) = 0$, we obtain[§§] then

$$U(r) = \tanh\left(\frac{1-r}{\delta}\right) + (1-\tanh(\delta^{-1})) \times \left(1 + r + \frac{1+\tanh(\delta^{-1})}{\delta} r\right)(1-r) \tag{C1}$$

with the properties, for small δ,

$$\begin{aligned}
U''(0) &= -8\delta^{-2}\mathrm{e}^{-2\delta^{-1}}\left(1+\delta+\frac{1}{2}\delta^2\right) + \cdots = O(\delta^{-2}\mathrm{e}^{-2\delta^{-1}}),\\
U'(1) &= -\delta^{-1} - 4\delta^{-1}\mathrm{e}^{-2\delta^{-1}} + \cdots \simeq -\delta^{-1},\\
U(1-\delta) &= \tanh(1) - 4\mathrm{e}^{-2\delta^{-1}} + \cdots \simeq 0.7616,\\
U(1-3\delta) &= \tanh(3) - 12\mathrm{e}^{-2\delta^{-1}} + \cdots \simeq 0.995,\\
\delta_{\mathrm{disp}} &= \int_0^1 (1-U(r)) r \,\mathrm{d}r = \ell_n(2)\delta - \frac{1}{24}\pi^2\delta^2 + \cdots \simeq 0.69315\delta,\\
\delta_{\mathrm{mom}} &= \int_0^1 U(r)(1-U(r)) r \,\mathrm{d}r = (1-\ell_n(2))\delta - \left(\ell_n(2) - \frac{1}{24}\pi^2\right)\delta^2 + \cdots \simeq 0.30685\delta
\end{aligned}$$

With $u_0(0) = \tau$ and $u_0(1) = \tau - \sigma$, more general profiles are created by

$$u_0(r) = \tau - \sigma + \sigma U(r) \tag{C2}$$

Acknowledgments

We want to acknowledge the interest, advice, and help of colleagues Han Slot (for suggestions on the Galerkin projection), Michiel Hochstenbach (for the fruitful discussions and suggestions on the nonlinear eigenvalue solver), Mark Peletier (the useful suggestions for the $Z = 0$ problem), and Pieter Sijtsma (for suggestions on the rotor-alone modes) and students Rik Rutjens (for suggestions on the Gauss–Legendre method) and Matthijs van Raaij.

References

[1] Rienstra, S. W., and Hirschberg, A., *An Introduction to Acoustics*, Technische Univ. Eindhoven, Eindhoven, The Netherlands, Extended and revised edition of IWDE 92-06, 2004, http://www.win.tue.nl/~sjoerdr/papers/boek.pdf [retrieved 1 Oct. 2019].

[2] Rienstra, S. W., *Fundamentals of Duct Acoustics*, VKI Lecture Series 2016-02, Notes of Course Progress in Simulation, Control and Reduction of Ventilation Noise, Von Karman Institute for Fluid Dynamics, Belgium, Nov. 2015.

[3] Tyler, J. M., and Sofrin, T. G., "Axial Flow Compressor Noise Studies," *Transactions of the Society of Automotive Engineers*, Vol. 70, 1962, pp. 309–332. https://doi.org/10.4271/620532

[4] Sofrin, T. G., and Cicon, D. E., "Ducted Fan Noise Propagation in Non-Uniform Flow—Part I: Test Background and Simplified Model," *11th AIAA Aeroacoustics Conference*, AIAA Paper 1987-2701, Oct. 1987. https://doi.org/10.2514/6.1987-2701

[5] Sofrin, T. G., and Cicon, D. E., "Ducted Fan Noise Propagation in Non-Uniform Flow—Part II: Wave Equation Solution," *11th AIAA Aeroacoustics Conference*, AIAA Paper 1987-2702, Oct. 1987. https://doi.org/10.2514/6.1987-2702

[§§] We could continue with more terms to make higher derivatives in $r = 0$ also equal to zero.

[6] Watson, W. R., and Jones, M. G., "Impedance Eduction in a Duct Using Linearized Euler Equations," *24th AIAA/CEAS Aeroacoustics Conference*, AIAA Paper 2018-3442, June 2018. https://doi.org/10.2514/6.2018-3442

[7] Nark, D. M., Jones, M. G., and Piot, E., "Assessment of Axial Wave Number and Mean Flow Uncertainty on Acoustic Liner Impedance Eduction," *24th AIAA/CEAS Aeroacoustics Conference*, AIAA Paper 2018-3444, June 2018. https://doi.org/10.2514/6.2018-3444

[8] Rienstra, S. W., "A Classification of Duct Modes Based on Surface Waves," *Wave Motion*, Vol. 37, No. 2, 2003, pp. 119–135. https://doi.org/10.1016/S0165-2125(02)00052-5

[9] Brambley, E. J., and Peake, N., "Classification of Aeroacoustically Relevant Surface Modes in Cylindrical Lined Ducts," *Wave Motion*, Vol. 43, No. 4, 2006, pp. 301–310. https://doi.org/10.1016/j.wavemoti.2006.01.001

[10] Brambley, E. J., "Surface Modes in Sheared Boundary Layers over Impedance Linings," *Journal of Sound and Vibration*, Vol. 332, No. 16, 2013, pp. 3750–3767. https://doi.org/10.1016/j.jsv.2013.02.028

[11] Brambley, E. J., "Fundamental Problems with the Model of Uniform Flow over Acoustic Linings," *Journal of Sound and Vibration*, Vol. 322, Nos. 4–5, 2009, pp. 1026–1037. https://doi.org/10.1016/j.jsv.2008.11.021

[12] Rienstra, S. W., and Darau, M., "Boundary Layer Thickness Effects of the Hydrodynamic Instability along an Impedance Wall," *Journal of Fluid Mechanics*, Vol. 671, March 2011, pp. 559–573. https://doi.org/10.1017/S0022112010006051

[13] Pridmore-Brown, D., "Sound Propagation in a Fluid Flowing Through an Attenuating Duct," *Journal of Fluid Mechanics*, Vol. 4, No. 4, 1958, pp. 393–406. https://doi.org/10.1017/S0022112058000537

[14] Myers, M. K., "Transport of Energy by Disturbances in Arbitrary Steady Flows," *Journal of Fluid Mechanics*, Vol. 226, May 1991, pp. 383–400. https://doi.org/10.1017/S0022112091002434

[15] Ingard, K. U., "Influence of Fluid Motion Past a Plane Boundary on Sound Reflection, Absorption, and Transmission," *Journal of the Acoustical Society of America*, Vol. 31, No. 7, 1959, pp. 1035–1036. https://doi.org/10.1121/1.1907805

[16] Myers, M. K., "On the Acoustic Boundary Condition in the Presence of Flow," *Journal of Sound and Vibration*, Vol. 71, No. 3, 1980, pp. 429–434. https://doi.org/10.1016/0022-460X(80)90424-1

[17] Brambley, E. J., "Well-Posed Boundary Condition for Acoustic Liners in Straight Ducts with Flow," *AIAA Journal*, Vol. 49, No. 6, 2011, pp. 1272–1282. https://doi.org/10.2514/1.J050723

[18] Rienstra, S. W., and Vilenski, G. G., "Spatial Instability of Boundary Layer Along Impedance Wall," *14th AIAA/CEAS Aeroacoustics Conference*, AIAA Paper 2008-2932, May 2008. https://doi.org/10.2514/6.2008-2932

[19] Reed, M., and Simon, B., "Functional Analysis," *Methods of Modern Mathematical Physics*, Vol. 1, Academic Press, San Diego, CA, 1980.

[20] Brambley, E. J., Rienstra, S. W., and Darau, M., "The Critical Layer in Linear-Shear Boundary Layers over Acoustic Linings," *Journal of Fluid Mechanics*, Vol. 710, Nov. 2012, pp. 545–568. https://doi.org/10.1017/jfm.2012.376

[21] Vilenski, G. G., and Rienstra, S. W., "On Hydrodynamic and Acoustic Modes in a Ducted Shear Flow with Wall Lining," *Journal of Fluid Mechanics*, Vol. 583, July 2007, pp. 45–70. https://doi.org/10.1017/S0022112007006106

[22] Vilenski, G. G., and Rienstra, S. W., "Numerical Study of Acoustic Modes in Ducted Shear Flow," *Journal of Sound and Vibration*, Vol. 307, Nos. 3–5, 2007, pp. 610–626. https://doi.org/10.1016/j.jsv.2007.06.045

[23] Oppeneer, M., Rienstra, S. W., Lazeroms, W., Mattheij, R. M. M., and Sijtsma, P., "Acoustic Modes in a Duct with Slowly Varying Impedance and Non-Uniform Mean Flow and Temperature," *17th AIAA/CEAS Aeroacoustics Conference*, AIAA Paper 2011-2871, June 2011. https://doi.org/10.2514/6.2011-2871

[24] Oppeneer, M., Rienstra, S. W., and Sijtsma, P., "Efficient Mode-Matching Based on Closed Form Integrals of Pridmore-Brown Modes," *AIAA Journal*, Vol. 54, No. 1, 2016, pp. 266–279. https://doi.org/10.2514/1.J054167

[25] Goldstein, M. E., and Rice, E., "Effect of Shear on Duct Wall Impedance," *Journal of Sound and Vibration*, Vol. 30, No. 1, 1973, pp. 79–84. https://doi.org/10.1016/S0022-460X(73)80051-3

[26] Abramowitz, M., and Stegun, I. A., *Handbook of Mathematical Functions*, National Bureau of Standards, Dover, New York, 1964.

[27] Bandres, M. A., Gutiérrez-Vega, J. C., and Chávez-Cerda, S., "Parabolic Nondiffracting Optical Wavefields," *Optics Letters*, Vol. 29, No. 1, 2004, pp. 44–46. https://doi.org/10.1364/OL.29.000044

[28] Bandres, M. A., and Rodrguez-Lara, B. M., "Nondiffracting Accelerating Waves: Weber Waves and Parabolic Momentum," *New Journal of Physics*, Vol. 15, No. 1, 2013, Paper 013054. https://doi.org/10.1088/1367-2630/15/1/013054

[29] Rienstra, S. W., "Sound Propagation in Slowly Varying 2D Duct with Shear Flow," *22nd AIAA/CEAS Aeroacoustics Conference*, AIAA Paper 2016-2925, May–June 2016. https://doi.org/10.2514/6.2016-2925

[30] Khorrami, M. R., Malik, M. R., and Ash, R. L., "Application of Spectral Collocation Techniques to the Stability of Swirling Flows," *Journal of Computational Physics*, Vol. 81, No. 1, 1989, pp. 206–229. https://doi.org/10.1016/0021-9991(89)90071-5

[31] Cooper, A. J., and Peake, N., "Propagation of Unsteady Disturbances in a Slowly Varying Duct with Mean Swirling Flow," *Journal of Fluid Mechanics*, Vol. 445, Oct. 2001, pp. 207–234. https://doi.org/10.1017/S0022112001005559

[32] Brambley, E. J., and Peake, N., "Sound Transmission in Strongly Curved Slowly Varying Cylindrical Ducts with Flow," *Journal of Fluid Mechanics*, Vol. 596, Jan. 2008, pp. 387–412. https://doi.org/10.1017/S0022112007009603

[33] Boyer, G., Piot, E., and Brazier, J.-P., "Theoretical Investigation of Hydrodynamic Surface Mode in a Lined Duct with Sheared Flow and Comparison with Experiment," *Journal of Sound and Vibration* Vol. 330, No. 8, 2011, pp. 1793–1809. https://doi.org/10.1016/j.jsv.2010.10.035

[34] Lloyd, A. E. D., and Peake, N., "The Propagation of Acoustic Waves in a Slowly Varying Duct with Radially Sheared Axial Mean Flow," *Journal of Sound and Vibration*, Vol. 332, No. 17, 2013, pp. 3937–3946. https://doi.org/10.1016/j.jsv.2013.02.038

[35] Mehrmann, V., and Voss, H., "Nonlinear Eigenvalue Problems: A Challenge for Modern Eigenvalue Methods," *GAMM-Mitteilungen*, Vol. 27, No. 2, 2004, pp. 121–152. https://doi.org/10.1002/gamm.201490007

[36] Mohseni, K., and Colonius, T., "Numerical Treatment of Polar Coordinate Singularities," *Journal of Computational Physics*, Vol. 157, No. 2, 2000, pp. 787–795. https://doi.org/10.1006/jcph.1999.6382

[37] Boyd, J. P., *Chebyshev and Fourier Spectral Methods*, Dover, New York, 2000.

[38] Aubin, J.-P., *Approximation of Elliptic Boundary-Value Problems*, Wiley-Interscience, New York, 1972.

[39] Ern, A., and Guermond, J.-L., *Theory and Practice of Finite Elements*, Springer–Verlag, New York, 2004.

[40] Mattheij, R. M. M., Rienstra, S. W., and ten Thije Boonkkamp, J. H. M., *Partial Differential Equations: Modeling, Analysis, Computation, (SIAM monographs on Mathematical Modeling and Computation)*, Vol. 10, Soc. for Industrial and Applied Mathematics, Philadelphia, 2005.

[41] Bender, C. M., and Orszag, S. A., *Advanced Mathematical Methods for Scientists and Engineers*, McGraw–Hill, New York, 1978.

[42] Goldstein, M. E., *Aeroacoustics*, McGraw–Hill, New York, 1976.

C. Bailly
Associate Editor